


# Inhibiting atrial natriuretic peptide clearance reduces myocardial fibrosis and improves cardiac function in diabetic rats

Jules Joel Bakhos<sup>1,‡</sup>, Youakim Saliba<sup>1,‡</sup>, Joelle Hajal<sup>1</sup>, Guy Achkouty<sup>1</sup>, Hrag Oskaridjian<sup>1</sup>, Miguel Albuquerque<sup>2,3</sup>, Chloé Azevedo<sup>4</sup>, Albert Semaan<sup>1</sup>, Nadine Suffee<sup>4</sup>, Elise Balse<sup>4</sup>, Stéphane N. Hatem<sup>4,\*</sup>, and Nassim Fares <sup>1,\*</sup>

<sup>1</sup>Laboratory of Research in Physiology and Pathophysiology, Faculty of Medicine, Saint-Joseph University of Beirut, 17-5208 - Mar Mikhaël, Beirut 1104 2020, Lebanon; <sup>2</sup>INSERM, Centre de Recherche sur L'inflammation, UMR 1149, Université Paris-Cité, 45 Rue des Saints-Pères 75006 Paris, France; <sup>3</sup>Service d'Anatomie Pathologique, Hôpital Beaujon, Assistance Publique-Hôpitaux de Paris, 100 Bd du Général Leclerc, 92110 Clichy, France; and <sup>4</sup>Institute of Cardiometabolism and Nutrition, IHU ICAN, Sorbonne University, INSERM UMR\_S1166 Pitié-Salpêtrière Hospital, 47-83 boulevard de l'Hôpital, 75013 Paris, France

Received 14 October 2024; revised 6 March 2025; accepted 10 March 2025; online publish-ahead-of-print 19 March 2025

Handling Editor: Daniel Ketelhuth

## Aims

Natriuretic peptides (NPs) exert pleiotropic effects through the recruitment of cyclic guanosine monophosphate (cGMP) signalling pathways depending on their bioavailability, which is regulated by clearance receptors and peptidases. Here, we tested the hypothesis that increasing myocardial bioavailability of NP has a beneficial effect on heart failure. We studied the effects of a mutated NP, M-atrial natriuretic peptide (MANP), resistant to neprilysin in a model of diabetic cardiomyopathy characterized by marked myocardial fibrosis.

## Methods and results

Natriuretic peptides as well as sacubitril were delivered via osmotic mini-pumps to high-fat/streptozotocin-induced Type 2 diabetic (T2D) rats. Cardiac function was evaluated by echocardiography. Myocardial remodelling was studied by histological approaches, collagen phenotype, and atrial natriuretic peptide (ANP)/cGMP concentrations. Live-cell cGMP biosensing was conducted on cultured rat cardiac fibroblasts to investigate the biological effects of NP. Cyclic guanosine monophosphate signalling pathway was studied using multiple antibody arrays and biochemical assays in cardiac tissue and cultured fibroblasts. M-atrial natriuretic peptide exhibits superior efficacy than ANP in reducing left ventricular dysfunction and myocardial fibrosis with less extracellular matrix deposition. *In vitro*, MANP and ANP similarly generated cGMP and activated the protein kinase G (PKG) signalling pathway in cardiac fibroblasts, attenuating Mothers against decapentaplegic homolog 2 (SMAD) activation, collagen secretion, and cell proliferation. Nevertheless, *in vivo*, MANP specifically enhanced cardiac cGMP accumulation and was more potent than ANP in activating myocardial cGMP/PKG signalling and inhibiting the profibrotic SMAD, extracellular signal-regulated kinases 1/2, and nuclear factor of activated T cells 3 pathways. Endopeptidase inhibition using sacubitril also led to cardiac ANP/cGMP accumulation and reduced myocardial fibrosis.

## Conclusion

Myocardial bioavailability of ANP is a major determinant of peptide efficacy in reducing cardiac fibrosis and improving pump function during diabetic cardiomyopathy.

## Keywords

Mutated atrial natriuretic peptide • Diabetes • Cardiomyopathy • Cardiac fibrosis • cGMP/PKG

\* Corresponding authors. Tel: +9613131950, Email: [nassim.fares@usj.edu.lb](mailto:nassim.fares@usj.edu.lb) (N.F.); Tel: +33682403356, Email: [s.hatem@ihuican.org](mailto:s.hatem@ihuican.org) (S.N.H.)

‡ The first two authors are co-first authors to the study.

© The Author(s) 2025. Published by Oxford University Press on behalf of the European Society of Cardiology.

This is an Open Access article distributed under the terms of the Creative Commons Attribution-NonCommercial License (<https://creativecommons.org/licenses/by-nc/4.0/>), which permits non-commercial re-use, distribution, and reproduction in any medium, provided the original work is properly cited. For commercial re-use, please contact [reprints@oup.com](mailto:reprints@oup.com) for reprints and translation rights for reprints. All other permissions can be obtained through our RightsLink service via the Permissions link on the article page on our site—for further information please contact [journals.permissions@oup.com](mailto:journals.permissions@oup.com).

## Translational perspective

Myocardial bioavailability of natriuretic peptides is crucial for mitigating cardiac fibrosis and improving cardiac function in diabetic cardiomyopathy and heart failure in general. M-atrial natriuretic peptide holds the potential as a new treatment modality in the management of heart failure.

## Introduction

Natriuretic peptides (NPs) initially recognized to regulate sodium and volume homeostasis and, hence, protect against high blood pressure, also show a range of beneficial effects on the heart, vessels, and kidneys. They can also influence glucose metabolism and regulate adipose tissue distribution, lipolysis, and metabolic activity.<sup>1,2</sup> The pleiotropic effects of NP are primarily mediated by cyclic guanosine monophosphate (cGMP) second messengers that are recruited following NP binding on Type A or Type B plasma membrane NP receptors that are widely expressed. Furthermore, the biological effects of NP depend on their half-life, 3 min for atrial natriuretic peptide (ANP) and 20 min for brain natriuretic peptide (BNP), which is regulated by clearance receptor (NPR-C) and a variety of peptidases, including neprilysin (NEP).<sup>3</sup>

Various pharmacological strategies have been developed to modulate the NP system, notably in the context of heart failure, characterized by altered cGMP pathway.<sup>4,5</sup> For instance, human recombinant NPs such as carperitide (for ANP) and nesiritide (for BNP) have been investigated for heart failure treatment, with, however, controversial clinical outcomes.<sup>6</sup> Another strategy has been pioneered by decreasing ANP elimination through neutral endopeptidase NEP inhibition. This leads to enhanced bioavailability of ANP that otherwise required continuous infusion of the peptide at a low dose.<sup>3</sup> Sacubitril (SACU)/valsartan is the first-in-class agent combining NEP inhibitor and angiotensin receptor blocker that has been shown to improve cardiovascular outcomes, myocardial performance, and reduced hospitalization and mortality of heart failure patients.<sup>7–11</sup> In addition to NP, NEP hydrolyzes several hormones such as bradykinin, angiotensin I and II, and endothelin that could contribute to the systemic and local effects of enzyme inhibition on cardiovascular and kidney axes.<sup>12</sup> Undoubtedly, the precise pharmacological properties and mechanisms of action of NP as well as related pharmacological molecules remain to be determined.

One current hypothesis stipulates that depending on their tissue bioavailability, NP can have marked local tissular effects contributing to the reduction of myocardial hypertrophic and fibrotic remodelling.<sup>1,2</sup> This hypothesis was tested here using a mutated isoform of ANP, M-atrial natriuretic peptide (MANP), resistant to NEP degradation<sup>13,14</sup> with a superior bioavailability and efficacy as to ANP.<sup>15,16</sup> Not only is MANP resistant to NEP degradation but to insulin-degrading enzyme (IDE) also with an IC<sub>50</sub> that is 30-fold higher than ANP.<sup>13,14</sup> Indeed, MANP is actively under clinical investigation for resistant and essential hypertension treatment.<sup>17–20</sup>

Herein, we used the high-fat/streptozotocin (STZ)-induced Type 2 diabetes (T2D) model that reproduces the diabetic cardiomyopathy notably characterized by diastolic dysfunction and marked myocardial fibrosis.<sup>21–26</sup> We provide novel evidence that modulating peptide bioavailability determines the effects of ANP on cardiac fibrosis.

## Methods

### Animal euthanasia

The euthanasia of rats in this study was performed in accordance with the most recent American Veterinary Medical Association Guidelines for the Euthanasia of Animals 2020 Edition. The procedure involved the intraperitoneal administration of a combination of ketamine (100 mg·kg<sup>-1</sup>; Panpharma, Luitré, France) and xylazine (10 mg·kg<sup>-1</sup>; Interchemie, Waalre, Holland) to ensure rapid and painless unconsciousness. After

confirmation of deep anaesthesia, by the absence of pedal withdrawal reflex, the animals were euthanized by bilateral thoracotomy and exsanguination through heart excision to ensure a quick and humane death.

### Diabetes animal model and treatments

The study was carried out on male Wistar rats aged 12 months and weighing 450 ± 25 g. The conventional high-fat diet combined with STZ (Sigma-Aldrich, St Louis, MO, USA) injections was used to induce T2D. Rats were fed a high-fat diet (60% kcal from lard) for 4 weeks before receiving three intraperitoneal STZ injections (40 mg·kg<sup>-1</sup>) on three consecutive days. Streptozotocin was diluted with a citrate buffer at pH 4.5. Sham animals received citrate injections. To guarantee proper diabetes induction, blood glucose levels were measured 72 h following the third STZ injection. After a 12-h fast, conscious rats were placed in rodent plexiglass restrainers (IITC Life Science Inc., CA, USA), and blood glucose levels were measured from the tail using a glucometer (Accu-Chek, Roche Diabetes Care, IN, USA). The tails were first cleaned with 70% alcohol, and measurements were taken with the second drop of blood. Diabetic animals had blood glucose levels higher than 200 mg·dL<sup>-1</sup>. Under ketamine/xylazine (50 and 10 mg·kg<sup>-1</sup>) anaesthesia, osmotic mini-pumps (model 2004; Alzet, Durect, CA, USA) were implanted subcutaneously on the back posterior to the scapulae. The pumps delivered 0.25 µL·h<sup>-1</sup> and a dosage of 2 pmol·kg<sup>-1</sup>·min<sup>-1</sup> of ANP or MANP (AnaSpec, Fremont, CA, USA) diluted in sterile 0.9% NaCl. Prior research has shown that these concentrations produce slight increases in diuresis but have little effect on systemic haemodynamics.<sup>15</sup> However, it is important to note that rats exhibit a higher metabolic rate compared with mongrel dogs. This difference suggests that, at the same weight-adjusted dose, ANP turnover and clearance in rats are expected to be higher leading to less changes in circulating and tissue concentrations of ANP and cGMP upon treatments. Sacubitril sodium (MedKoo Biosciences Inc., Durham, NC, USA) was administered in drinking water at a dose of 18 mg·kg<sup>-1</sup>·day<sup>-1</sup>, corresponding to a human equivalent dose of 2.85 mg·kg<sup>-1</sup>·day<sup>-1</sup> (≈97 mg SACU from the Entresto® twice daily recommended maintenance dose for an adult weighing 70 kg). To ensure that each rat received the intended dose of 18 mg·kg<sup>-1</sup>·day<sup>-1</sup>, we conducted a preliminary assessment 1 week before the protocol started, where we monitored individual water intake in metabolic cages (single housing) and in grouped housing conditions. Our results showed no significant difference in water consumption between the two conditions, suggesting that grouped housing did not affect individual intake. We opted for grouped housing for both practical and ethical reasons. Group housing is more feasible in long-term experiments, and importantly, it reduces stress and anxiety, which are known confounding factors in diabetic rodent models.

The animals were randomly assigned to two independent sets of experiments, the first set consisting of four groups (*n* = 6 each): Sham, T2D, T2D ANP, T2D MANP, and the second set consisting of five groups: Sham (*n* = 7), T2D (*n* = 6), T2D ANP (*n* = 5), T2D sacubitril (*n* = 7), and T2D ANP SACU (*n* = 6). The duration of the treatments was 6 weeks after diabetes establishment. Before the end of the protocol, rats were individually housed for 24 h in metabolic cages to assess for urine output, water and food intake. At the end of the protocol, rats were euthanized as previously described, and blood and hearts were collected for further studies. Each heart was cut into five cross-sectional parts, dedicated for histology (in formalin), western blots and arrays, collagen assays, and ANP/cGMP measurements. The latter four parts were flash frozen in liquid nitrogen and then kept at -80°C.

### Echocardiography

The high-resolution colour Doppler ultrasound system SonoScape S2V (SonoScape Co., Shenzhen, China) with a 9 MHz C611 transducer intended for mice and rats was used to perform transthoracic echocardiography. An

EZ-SA800 Anesthesia Single Animal System (E-Z Systems, PA, USA) was used to anaesthetize the rats prior to sacrifice. The dose of isoflurane (Baxter, Deerfield, IL, USA) used was 5% for induction and 3% for maintenance, with a flow rate of 1 L·min<sup>-1</sup>. The parasternal long-axis 2D view of the left ventricle was captured in M-mode at the level of the papillary muscles to assess the thickness of the ventricular walls and internal diameters, enabling calculations of fractional shortening (FS) and ejection fraction (EF) using the Teichholz method. This procedure was carried out by two independent operators who were unaware of the experimental conditions. All measurements were taken between 9 a.m. and noon, with duplicate readings acquired for each condition.

## Rat ventricular cardiac fibroblast isolation and culture

A group of normal Wistar rats ( $n = 5$ ) were assigned for the *in vitro* studies and euthanized as previously described. Hearts were excised and ventricles were placed in ice-cold modified Tyrode solution with the following composition (in mM): 117 NaCl, 5.7 KCl, 1.7 MgCl<sub>2</sub>, 4.4 NaHCO<sub>3</sub>, 1.5 KH<sub>2</sub>PO<sub>4</sub>, 10 HEPES, 10 creatine monohydrate, 20 taurine, 11.7 D-glucose, and 1% bovine serum albumin, adjusted to pH 7.1 with NaOH. Ventricles were minced and subjected to four rounds of enzymatic digestion using modified Tyrode solutions: collagenase Type V (165.1 U/mL) and protease Type XXIV (4.62 U/mL) from Sigma-Aldrich, St. Louis, MO, USA, for 20 min at the beginning, and collagenase Type V (157 U/mL) for three more 20-min rounds. Supernatants from each bath were pooled, and enzymatic reaction was stopped by adding cold foetal bovine serum. After centrifugation at 500 rpm for 10 min, the cardiomyocytes were eliminated, and the non-myocyte cells were separated by centrifugation at 2000 rpm for 10 min. The cells were then suspended in Dulbecco's modified Eagle's medium, supplemented with 1% penicillin/streptomycin and 10% heat-inactivated foetal bovine serum from Sigma-Aldrich, St. Louis, MO, USA. After incubating for 2 h, non-adherent cells were discarded, and the remaining adherent fibroblasts were rinsed with fresh culture medium. Cells were counted and equally dispatched to maintain consistency across conditions. After 24 h, cells had the fibroblast-like fusiform and spindle morphology. Cells were studied after 5 days of culture. A subset of cells was treated for 24 h with high glucose to mimic hyperglycaemia with or without ANP and MANP (100 pM). Six cultures were performed for the MTT and collagen secretion assays, western blots, and cGMP live-cell imaging; for each culture, all the experiments were performed.

## Cyclic guanosine monophosphate live-cell imaging

Live cultured cardiac fibroblasts were used to monitor cGMP synthesis. This was done by utilizing a Genetically Encoded Nucleotide Indicator (GENle) that carried mNeonGreen, a highly luminous monomeric green fluorescent protein. The GENle (Montana Molecular, MT, USA) is a sensor that exhibits a strong initial fluorescence that decreases as the intracellular cGMP levels increase. Experiments were conducted following the manufacturer's protocol. After cell synchronization on Day 3 of culture, the cells were exposed to a BacMam-modified baculovirus along with sodium butyrate, an histone deacetylase inhibitor that is essential to sustaining viral expression. After 24 h of infection, the cell culture medium was replaced, and the cells were left for an additional 24 h. The cells were placed in the modified Tyrode solution and left to incubate for 15 min prior to starting the recordings. Cells were acutely perfused with the different peptides using a ValveLink8.2 Perfusion Controller (Automate Scientific, CA, USA). Images were acquired and analysed using a digital fluorescent imaging system (InCyt Im2; Intracellular Imaging Inc., Cincinnati, OH, USA). To generate quantification histograms, analysis was done at the 3600-s time point vs. the time of ANP/MANP addition.

## Cardiac and plasma atrial natriuretic peptide/cyclic guanosine monophosphate measurement

Animals were euthanized as previously described. Blood was collected from each animal group into EDTA tubes and centrifuged at 4500 rpm for 10 min to separate plasma. ANP and cGMP plasma concentrations were measured

using enzyme-linked immunosorbent assay (ELISA) kits according to the manufacturers' instructions (Rat Atrial Natriuretic Peptide ANP ELISA Kit; CSB-E12982; Cusabio, Houston, TX, USA; and Cyclic GMP Complete ELISA Kit; ab133052; Abcam, Cambridge, UK). To measure ventricular ANP and cGMP concentrations, cardiac tissues were first homogenized in either phosphate buffer system for ANP measurement or 0.1 M HCl for cGMP, before performing the test. Acetylation of the samples was carried out to improve the sensitivity of the cGMP assay.

## Antibody array and western blot

Ventricular tissue and cultured cardiac fibroblasts were homogenized and lysed in radioimmunoprecipitation assay buffer lysis buffer including protease and phosphatase inhibitors. Protein concentrations were measured using the Bradford protein assay (Bio-Rad, Marnes-la-Coquette, France), and samples were denatured in Laemmli loading buffer (Bio-Rad, Marnes-la-Coquette, France) containing 10%  $\beta$ -mercaptoethanol (Sigma-Aldrich, St. Louis, MO, USA) at 37°C for 20 min. Proteins were separated by SDS 12% PAGE and transferred to polyvinylidene fluoride membranes (Bio-Rad, Marnes-la-Coquette, France) blocked with 5% bovine serum albumin. The membranes were incubated overnight at 4°C with the corresponding primary antibodies: anti-PKG-I (protein kinase G) (ab90502; 1/1000), anti-VASP (vasodilator-stimulated phosphoprotein) (ab209093; 1/1000), anti-phospho-VASP Ser239 (ab194747; 1/500), anti-SMAD2 (Mothers against decapentaplegic homolog 2) (ab63576; 1/500), anti-phospho-SMAD2 S467 (ab53100; 1/500), anti-SMAD3 (mothers against decapentaplegic homolog 3) (ab28379; 1/500), and anti-phospho-SMAD3 S423 + S425 (ab52903; 1/500). Blots were re-probed for glyceraldehyde-3-phosphate dehydrogenase (GAPDH) (#5174; 1/2500) from Cell Signaling Technology, Danvers, MA, USA. Goat anti-rabbit (1/3000, Bio-Rad Laboratories, Marnes-la-Coquette, France) was used as the secondary antibody. An imaging system fitted with a CCD camera was used to detect enhanced chemiluminescence signals (Omega Lum G, Aplegen, Gel Company, SF, USA). Image Studio Lite Ver 5.2 (LI-COR Biosciences, Lincoln, NE, USA) was used to do the quantifications. For each condition, three western blots were used.

To generate antibody arrays, 5  $\mu$ g of proteins were immobilized onto polyvinylidene fluoride membranes using dot blot apparatus (Cleaver Scientific, Rugby, UK) before blocking and incubating with the primary antibody. The same GAPDH and secondary antibodies, with the rabbit anti-goat (1/3000, ab6741, Abcam), were utilized as in the western blot studies with the following additional antibodies: anti-Col1 (ab34710), anti-Col3 (ab7778), anti-calcineurin (sc-6124), anti-nuclear factor of activated T cells 3 (NFATc3) (sc-8321), anti-NFATc3 phospho S165 (ab59204), anti-nuclear factor of activated T cells 4 (NFATc4) (ab183117), anti-NFATc4 phospho S168/170 (sc-32630), anti-extracellular signal-regulated kinases 1/2 (ERK1/2) (#4695S), anti-ERK1/2 phospho Thr202/Tyr204 (#4370S), anti-stress-activated protein kinases (SAPK)/Jun amino-terminal kinases (JNK) (#9252S), anti-SAPK/JNK phospho Thr183/Tyr185 (#4668S), anti-P38 MAPK (#8690S), anti-P38 phospho Thr180/Tyr182 (#4511S), anti-IDE (sc-393887), and anti-CD10/NEP (sc-46656). ab is for Abcam, sc is for Santa Cruz Biotechnology (Dallas, TX, USA), and the remaining antibodies are from Cell Signaling Technology, Danvers, MA, USA.

## Histology and immunofluorescence

Formalin-fixed cardiac tissues were embedded in paraffin, cut into 4  $\mu$ m slices, and stained with Masson's trichrome or Sirius red (Sigma-Aldrich, St. Louis, Missouri, USA). Histological examinations were conducted by two independent pathologists, and fibrosis was assessed using a scoring procedure, an Aperio Slide Scanner and ImageScope software v12.4.6.5003 (Leica Biosystems, Wetzlar, Germany), and a VanGuard High-Definition Digital Camera (VEE GEE Scientific, IL, USA). Wheat germ agglutinin (WGA) staining was carried out in accordance with the manufacturer's instructions (Thermo Fisher Scientific, MA, USA). Platelet-derived growth factor receptor alpha (PDGFR $\alpha$ ) labelling was followed by antigen retrieval with HCl. Triton X-100 was used to permeabilize the membrane, and 10% goat serum and 1% bovine serum albumin were used for blocking. Platelet-derived growth factor receptor alpha antibody (ab124392; 1/100; Abcam, Cambridge, USA) was employed overnight at 4°C to detect fibroblasts. The secondary antibody was goat anti-rabbit IgG H&L Alexa Fluor 594 (ab150084; Abcam), which was pre-adsorbed in a column matrix

containing immobilized mouse serum proteins to reduce background by minimizing cross-reactivity with endogenous proteins and immunoglobulins. Sections were mounted with Fluoroshield Mounting Medium containing DAPI (Abcam, Cambridge, UK), and images were taken with an Axioskop 2 immunofluorescence microscope (Carl Zeiss Microscopy GmbH, Jena, Germany) outfitted with a CoolCube 1 CCD camera (MetaSystems, Newton, MA, USA). Images were analysed using ImageJ. Wheat germ agglutinin immunofluorescence on heart sections was quantified by analysing the fluorescent area fraction. First, images of stained heart sections were converted to greyscale and background noise subtracted to enhance signal specificity. The thresholding function was then applied to distinguish the WGA-positive regions from the background. The percentage of WGA-stained area relative to the total tissue area was then calculated.

## Soluble collagen and proliferation assays

MTT assay was used to analyse cell proliferation. The cell culture medium was withdrawn, and  $0.5 \text{ mg mL}^{-1}$  MTT Tyrode solution was added to the cells. After an hour of incubation at  $37^\circ\text{C}$ , the MTT solution was discarded, and the cells were rinsed with Tyrode. MTT formazan purple crystals were dissolved in 100% DMSO, and absorbance was measured at 550 nm.

The Sircol collagen test (Biocolor, County Antrim, UK) was used to measure soluble collagen. In brief, ventricular tissues were homogenized in an acid-pepsin solution, whereas cultured cell supernatants were used directly. Each sample and standard was then treated with the Sircol dye reagent. Collagen dye pellets were centrifuged, rinsed with acetic acid, and then dissolved in an alkali reagent. Absorbance was measured at 550 nm.

## Statistical analysis

All quantitative data are reported as mean  $\pm$  SEM with individual data points. Normal distribution and equal variance of the values were verified using the Shapiro–Wilk and Bartlett's tests, respectively. The groups that were compared were as follow: first set of experiments (Sham vs. T2D, T2D vs. T2D ANP, T2D vs. T2D MANP, and T2D ANP vs. T2D MANP) and second set of experiments (Sham vs. T2D, T2D vs. T2D ANP, T2D vs. T2D SACU, T2D vs. T2D ANP SACU, T2D ANP vs. T2D SACU, T2D ANP vs. T2D ANP SACU, and T2D SACU vs. T2D ANP SACU). Statistical analyses included repeated-measures two-way analysis of variance (ANOVA) followed by Sidak's test, one-way ANOVA followed by Sidak's or Holm–Sidak's test, Kruskal–Wallis with Dunn's test, and Brown–Forsythe and Welch ANOVA followed by Dunnett's T3. Statistical significance was denoted by \* $P < 0.05$ , \*\* $P < 0.01$ , \*\*\* $P < 0.001$ , and \*\*\*\* $P < 0.0001$ .

## Results

### M-atrial natriuretic peptide exhibits superior efficacy than atrial natriuretic peptide in reducing left ventricular dysfunction and fibrosis associated with Type 2 diabetes

In male rats subjected to STZ injections coupled to high-fat diet for 6 weeks, we compared the effects of low doses of ANP and MANP delivered subcutaneously by osmotic pumps on cardiac remodelling and dysfunction (Figure 1A). Three days after diabetes induction, animals showed high fasting plasma glucose ( $>200 \text{ mg dL}^{-1}$ ) as compared with Sham ( $<100 \text{ mg dL}^{-1}$ ). A further increase of fasting plasma glucose was noted at Week 6 ( $\approx 500 \text{ mg dL}^{-1}$ ). Similar plasma glucose patterns were observed in the other groups albeit fasting plasma glucose remained unchanged at Week 6 under ANP and MANP (Figure 1B). Cardiac mass was unaltered when normalized to body weight in all groups (Figure 1C). Echocardiographic analyses showed a trend towards LV dilation (Figure 1D–F) in T2D animals. As expected, left ventricular function was declined in T2D (EF  $\approx 75\%$ , FS  $\approx 37\%$  in T2D vs. EF  $\approx 95\%$ , FS  $\approx 63\%$  in Sham). Left ventricular dysfunction was moderately

improved under ANP (EF  $\approx 82\%$ , FS  $\approx 44\%$ ) and almost restored with MANP treatment (EF  $\approx 92\%$ , FS  $\approx 56\%$ ) (Figure 1G and H). Heart rate did not differ among the different groups (Figure 1I) neither the heart weight (see Supplementary material online, Figure S1A). Microscopically, T2D rats developed diffuse myocardial fibrosis depicted by Masson's trichrome with an expansion of extracellular matrix labelled by WGA and spread of activated PDGFR $\alpha^+$  cardiac fibroblasts (Figure 1J–L). M-atrial natriuretic peptide treatment showed superior efficacy than ANP in protecting rat hearts with  $\approx 80\%$  and  $75\%$  decrease in Masson's trichrome and WGA staining, respectively, as compared with  $\approx 50\%$  decrease with ANP (Figure 1J and K). In contrast, similar fibroblast labelling extent was noted under both peptides (Figure 1L). At the molecular level, MANP inhibited SMAD3 activation as indicated by  $\approx 55\%$  lower phosphorylation levels compared with T2D animals (Figure 1M). These results indicate that MANP more efficiently than ANP reduces cardiac dysfunction and myocardial fibrosis in T2D rats. Subsequently, cardiac collagen characterization was done by antibody arrays for the major two collagen isoforms, Collagens I and III as well as Sircol assay for newly synthesized soluble collagen. Cardiac Collagen III but not Collagen I increased in T2D (by  $\approx 55\%$ ) coupled to a decrease in soluble collagen (by  $\approx 30\%$ ), whereas ANP-treated groups showed opposite cardiac collagen profiles (decrease by  $\approx 30\%$  in Collagen III and increase by  $\approx 25\%$  in soluble collagen). Of note, MANP led to significant decreases in both forms of collagen (by  $\approx 50\%$  in Collagen III and by  $\approx 20\%$  in soluble collagen) (Figure 1N–P).

### M-atrial natriuretic peptide inhibits cardiac nuclear factor of activated T cells 3 and extracellular signal-regulated kinases 1/2 fibrotic signalling in Type 2 diabetes

M-atrial natriuretic peptide treatment modulated key fibrotic signalling pathways in T2D hearts. Our antibody array analysis revealed that, while NFATc3 and ERK1/2 were not significantly induced in T2D hearts, MANP still significantly reduced NFATc3 activation as shown by the increase in the phosphorylated inactivated protein levels compared with T2D controls, indicating a suppression of calcineurin-dependent fibrotic signalling (Figure 2A and B). Additionally, ERK1/2 activation, a crucial mediator of profibrotic responses, was markedly attenuated in MANP-treated T2D hearts, as shown by the decrease of the phosphorylated/total protein levels (pERK/ERK) (Figure 2A and B).

### Atrial natriuretic peptide and M-atrial natriuretic peptide similarly regulate cyclic guanosine monophosphate signalling pathway in cardiac fibroblasts

As the antifibrotic effect of ANP has been attributed mainly to its action on cardiac fibroblasts,<sup>27–29</sup> we examined whether difference in antifibrotic effect between ANP and MANP could be related to distinct effects on fibroblasts. The mNeon Green GENle system, delivered through BACMAM, was employed for cGMP biosensing in primary cultured cardiac fibroblasts. This downward-sensing system exhibits bright initial green fluorescence, which diminishes in response to increased intracellular cGMP levels. Upon  $100 \text{ pM}$  MANP or ANP acute addition, the biosensor's fluorescence gradually decreased with comparable  $F/F_0$  for both peptides (Figure 3A and B). In addition, MANP and ANP similarly decreased rat cardiac fibroblast proliferation (by  $\approx 20\%$ ) and collagen secretion (by  $\approx 30\%$ ) as demonstrated by MTT and Sircol assays (Figure 3C and D). Fibroblasts were subsequently subjected to a 24-h treatment with elevated glucose, replicating conditions of diabetic hyperglycaemia, w/o MANP, or ANP. Profibrotic SMAD2 was activated by high glucose but showed decreased phosphorylation levels



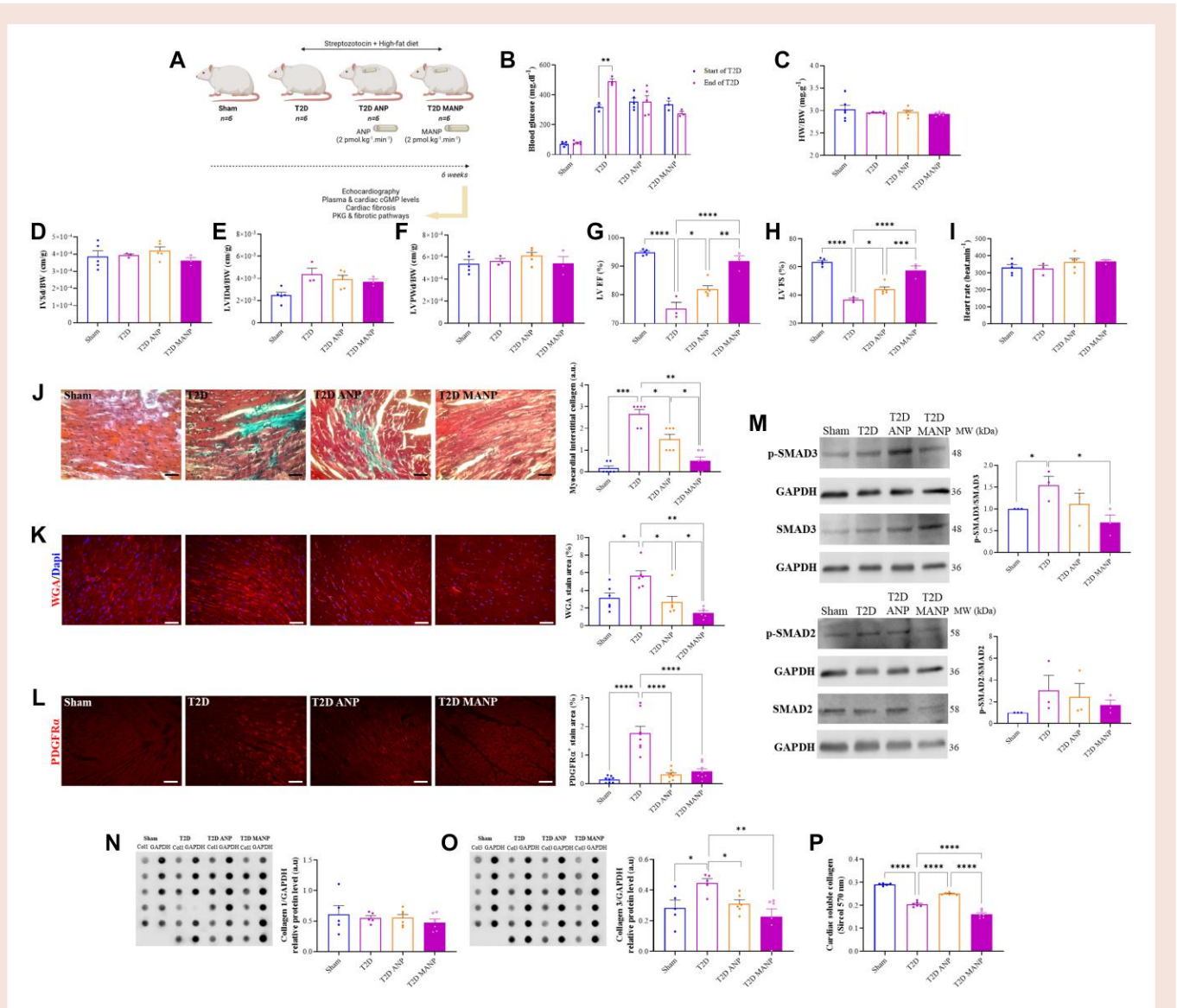


**Figure 1** Left ventricular remodelling in Type 2 diabetes is mitigated by M-atrial natriuretic peptide more effectively than atrial natriuretic peptide. (A) Experimental design for subjecting male rats to streptozotocin injections coupled to a high-fat diet as a model for Type 2 diabetes. Atrial natriuretic peptide and M-atrial natriuretic peptide were delivered by subcutaneous osmotic pumps at a dose of 2 pmol·kg<sup>-1</sup>·min<sup>-1</sup>. Cardiac function was assessed by echocardiography at 6 weeks of the protocol. Rats were then euthanized, and hearts and plasma were harvested for further histological and molecular analyses. Echocardiographic parameters were normalized to body weight to account for body size variation among the rats and interpret measurements independently of the individual animal's size. (B) Representative blood glucose in Sham, Type 2 diabetes, Type 2 diabetes atrial natriuretic peptide, and Type 2 diabetes M-atrial natriuretic peptide. (C) Mean heart weight over body weight ratio. (D) Mean interventricular septum thickness at end-diastole. (E) Mean left ventricular internal dimension at end-diastole. (F) Mean left ventricular posterior wall thickness at end-diastole. (G) Mean left ventricular ejection fraction. (H) Mean left ventricular fractional shortening. (I) Heart rate in all groups. (J–L) Representative heart sections for all groups showing Masson's trichrome staining, wheat germ agglutinin and platelet-derived growth factor receptor alpha immunofluorescence (594 nm; bar = 50 μm) with respective quantifications of analysed section areas. (M) Representative western blots and densitometric analyses of phosphorylated and total SMAD2/3 (each with glyceraldehyde-3-phosphate dehydrogenase as housekeeper protein) for all groups. (N, O) Antibody arrays for cardiac Collagens I and III using glyceraldehyde-3-phosphate dehydrogenase as internal control with respective quantifications for all groups. (P) Cardiac soluble collagen for all groups using Sircol assay. All quantitative data are reported as mean and individual data points ± SEM. Normal distribution of the values was checked by the Shapiro–Wilk test, and equal variance was checked by the Bartlett's test. Repeated-measures two-way analysis of variance followed by Sidak's test in B, one-way analysis of variance followed by Sidak's test in C–G, I, L–N, and P or Holm–Sidak's test in H and O, Kruskal–Wallis followed by Dunn's test in J, and Brown–Forsythe and Welch analysis of variance followed by Dunnett's T3 in K were performed. (B, D–I)  $n = 3$ –5 animals according to each bar points. (C, J)  $n = 6$  animals for each group. (K)  $n = 5$ –6 animals according to each bar points. (L)  $n = 4$  animals, each duplicate, for each group. (M)  $n = 3$  western blots from three animals for each group. (N, O)  $n = 5$ –6 animals according to each bar point ( $n = 1$  array). (P)  $n = 5$ –6 animals according to each bar points. \* $P < 0.05$ , \*\* $P < 0.01$ , \*\*\* $P < 0.001$ , and \*\*\*\* $P < 0.0001$ . ANP, atrial natriuretic peptide; GAPDH, glyceraldehyde-3-phosphate dehydrogenase; HW/BW, heart weight over body weight ratio; MANP, M-atrial natriuretic peptide; PDGFRα, platelet-derived growth factor receptor alpha; T2D, Type 2 diabetes; WGA, wheat germ agglutinin. The figure was created with BioRender.com.

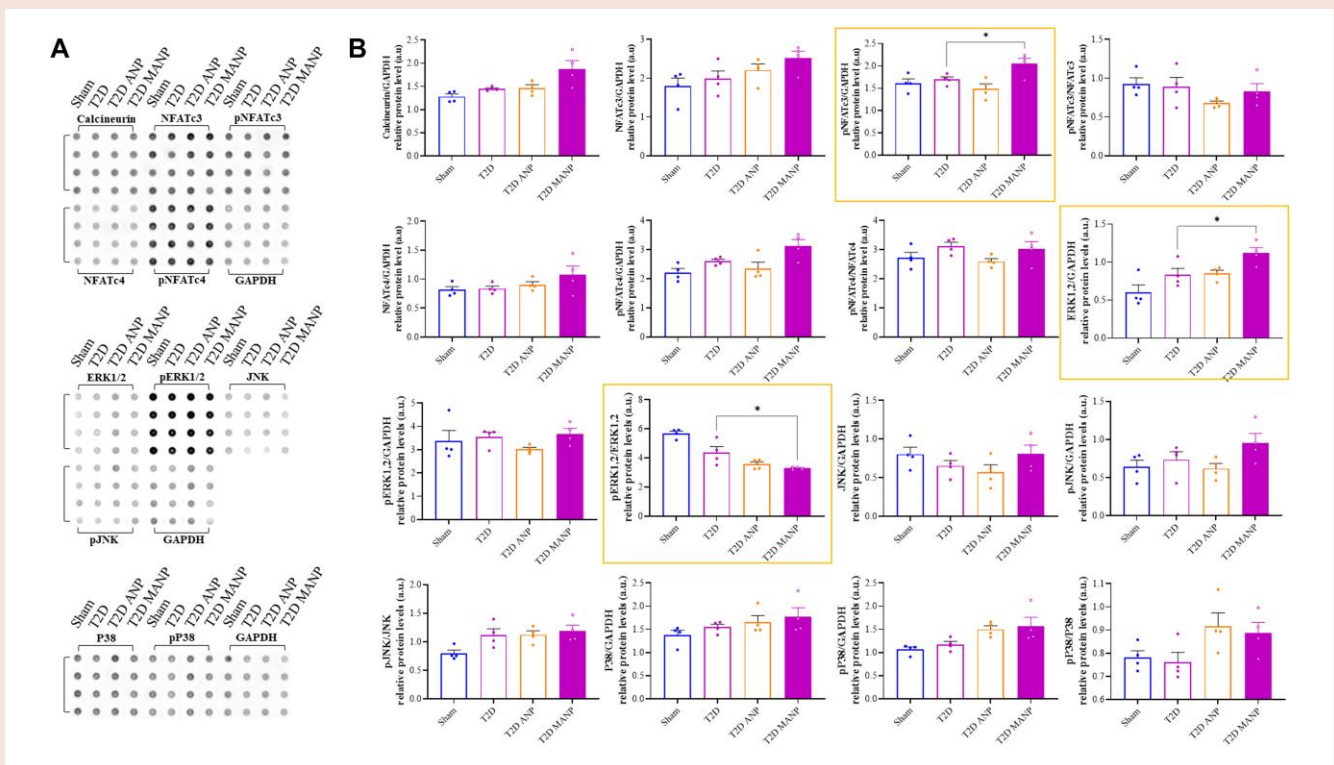


**Figure 2** M-atrial natriuretic peptide attenuates nuclear factor of activated T cells 3 and extracellular signal-regulated kinases 1/2 fibrotic signalling in Type 2 diabetes. (A) Antibody arrays for calcineurin, nuclear factor of activated T cells 3, phospho-nuclear factor of activated T cells 3, nuclear factor of activated T cells 4, phospho-nuclear factor of activated T cells 4, extracellular signal-regulated kinases 1/2, phospho-extracellular signal-regulated kinases 1/2, Jun amino-terminal kinases, phospho-Jun amino-terminal kinases, P38, and phospho-P38, using glyceraldehyde-3-phosphate dehydrogenase as internal control with respective quantifications (B) for all groups. All quantitative data are reported as mean and individual data points  $\pm$  SEM. Normal distribution of the values was checked by the Shapiro–Wilk test, and equal variance was checked by the Bartlett’s test. One-way analysis of variance followed by Sidak’s tests was performed.  $n = 4$  animals according to each bar point ( $n = 1$  array for each protein set). \* $P < 0.05$ . ANP, atrial natriuretic peptide; ERK1/2, extracellular signal-regulated kinases 1/2; GAPDH, glyceraldehyde-3-phosphate dehydrogenase; MANP, M-atrial natriuretic peptide; NFATc3, nuclear factor of activated T cells 3; NFATc4, nuclear factor of activated T cells 4; T2D, Type 2 diabetes. The figure was created with BioRender.com.

with both MANP and ANP (by  $\approx 55\%$ ) whereas SMAD3 remained stable (Figure 3E). High glucose inhibited cGMP-dependent pathway PKG/VASP as depicted by lower VASP phosphorylation levels at serine 239, whereas MANP/ANP activated this pathway in a comparable manner ( $\approx 2.3$ -fold) (Figure 3F). Therefore, ANP and MANP show the same biological properties on cardiac fibroblasts.

## M-atrial natriuretic peptide is more potent than atrial natriuretic peptide to activate cyclic guanosine monophosphate/protein kinase G signalling in the heart of Type 2 diabetic rats

We next examined whether differences in antifibrotic effect between wild-type and mutated ANP could be related to differences in peptide bioactivity, in line with the reduced clearance of the mutated peptide. Cardiac ANP concentration decreased ( $\approx 34\%$ ) whereas plasma ANP increased ( $\approx 1.9$ -fold) in T2D vs. Sham, with no noticeable effect for ANP treatment on both parameters (Figure 4A and B). M-atrial natriuretic peptide treatment increased cardiac ANP levels ( $\approx 2$ -fold vs. T2D) with a slight but non-significant increase in ANP plasma concentration ( $\approx 20\%$ ,  $P = 0.0967$ ) (Figure 4A and B). Additionally, myocardial concentration of cGMP was measured to evaluate the activation of

membrane particulate guanylate cyclase, which is triggered by NP. Cardiac but not plasma cGMP levels presented a tendency to decrease ( $\approx 50\%$ ,  $P = 0.13$ ) in T2D, which was attenuated in rats treated by ANP. In contrast, MANP treatment increased cardiac cGMP levels compared with all groups of rats ( $\approx 5$ -fold vs. T2D) as well as plasma cGMP albeit not as important as within the heart ( $\approx 2.9$ -fold vs. T2D) (Figure 4C and D). Furthermore, T2D inhibited cardiac cGMP-dependent pathway PKG/VASP as evidenced by lower VASP phosphorylation levels (by  $\approx 60\%$ ); both MANP and ANP treatments restored this pathway (Figure 4E). These results are consistent with more accumulation of MANP than ANP in the myocardium of T2D rats. To further dissect the relatively weak local cardiac effects of ANP, we checked the cardiac expression levels of the two endopeptidases that degrade ANP, i.e. IDE and NEP. Atrial natriuretic peptide but not MANP treatment led to a compensatory increase in cardiac IDE expression (Figure 4F and G).

## Endopeptidase inhibition using sacubitril reduces myocardial fibrosis in Type 2 diabetic rats

To further examine the impact of NP accumulation level in the myocardium on its antifibrotic effects, we inhibited the endopeptidase NEP using SACU (Figure 5A). First, T2D rats treated with SACU showed

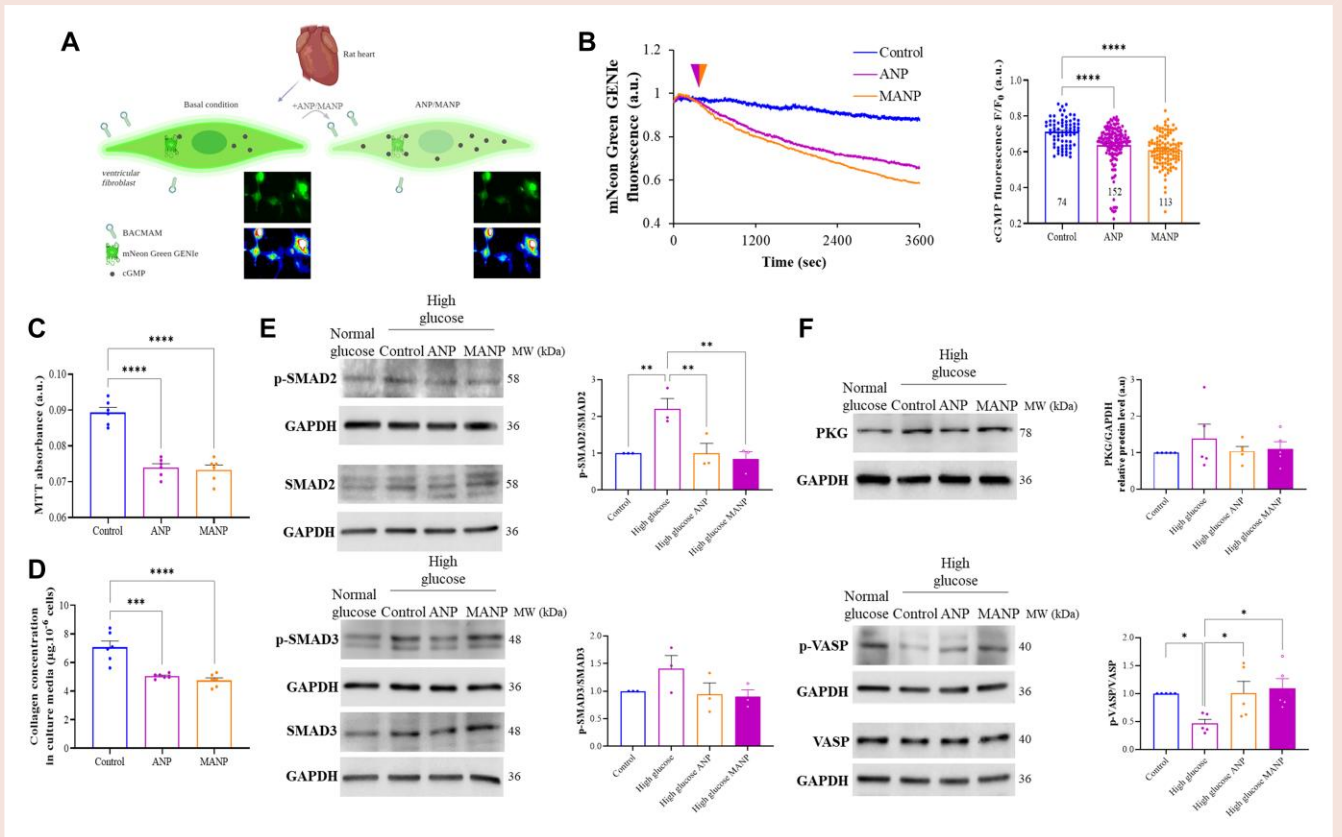


**Figure 3** M-atrial natriuretic peptide-driven protein kinase G activation and SMADs regulation in cardiac fibroblasts through cyclic guanosine monophosphate. (A) Illustration of the mNeon Green GENle system introduced through BACMAM for monitoring intracellular cyclic guanosine monophosphate in live primary cardiac fibroblasts. The emitted light from the probe exhibits an inverse relationship with cyclic guanosine monophosphate concentration. M-atrial natriuretic peptide or atrial natriuretic peptide was acutely introduced to the cells during imaging at a concentration of 100 pM. Cells were isolated from normal rat hearts. (B) Representative mNeon Green GENle probe fluorescence curves after the acute addition of M-atrial natriuretic peptide or atrial natriuretic peptide and  $F/F_0$  fluorescence quantifications conducted at the 3600-s time point vs. the time of atrial natriuretic peptide/M-atrial natriuretic peptide addition. (C, D) Proliferation and collagen secretion ( $\mu\text{g} \cdot 10^{-3}$  cells) of cultured rat cardiac fibroblasts treated for 24 h with 100 pM M-atrial natriuretic peptide or atrial natriuretic peptide, estimated by MTT and Sircol assays; absorbance at 570 nm. (E, F) Cultured rat cardiac fibroblasts were treated with high glucose for 24-h mimicking diabetic hyperglycaemia w/wo M-atrial natriuretic peptide or atrial natriuretic peptide. Representative western blots and densitometric analyses of phosphorylated and total SMAD2/3 and vasodilator-stimulated phosphoprotein, and protein kinase G (each with glyceraldehyde-3-phosphate dehydrogenase as housekeeper protein) are shown for all groups. All quantitative data are reported as mean and individual data points  $\pm$  SEM. Normal distribution of the values was checked by the Shapiro–Wilk test and equal variance was checked by the Bartlett’s test. One-way analysis of variance followed by Tukey’s test in B–D or Holm–Sidak’s test in E and F (lower panel) and Brown–Forsythe and Welch analysis of variance followed by Dunnett’s T3 in (F, upper panel) were performed. (B) A number of cells are presented for each bar; cells derive from six independent cultures. (C, D)  $n = 6$  independent cultures. (E)  $n = 3$  western blots from three independent cultures. (F)  $n = 5$  western blots from five independent cultures. \* $P < 0.05$ , \*\* $P < 0.01$ , \*\*\* $P < 0.001$ , and \*\*\*\* $P < 0.0001$ . ANP, atrial natriuretic peptide; ERK1/2, extracellular signal-regulated kinases 1/2; GAPDH, glyceraldehyde-3-phosphate dehydrogenase; MANP, M-atrial natriuretic peptide; NFATc3, nuclear factor of activated T cells 3; NFATc4, nuclear factor of activated T cells 4; PKG, protein kinase G; T2D, Type 2 diabetes; VASP, vasodilator-stimulated phosphoprotein. The figure was created with BioRender.com.

the same metabolic profiles as their counterparts (Figure 5B). Following diabetes induction, cardiac mass was unaltered when normalized to body weight in all groups (Figure 5C), and there was no significant cardiac dilation in all groups of rats (Figure 5D–F). Left ventricular function was reduced in T2D ( $\text{EF} \approx 78\%$ ,  $\text{FS} \approx 40\%$ ) and partially restored in ANP ( $\text{EF} \approx 85\%$ ,  $\text{FS} \approx 50\%$ ) and SACU ( $\text{EF} = 87\%$ ,  $\text{FS} \approx 50\%$ ) conditions, without an additional effect of the association of ANP and SACU ( $\text{EF} \approx 83\%$ ,  $\text{FS} \approx 44\%$ ) (Figure 5G and H). Heart rate did not differ among the different groups (Figure 5I) neither the heart weight (see Supplementary material online, Figure S2A). Comprehensive analysis of myocardial interstitial fibrosis was conducted using Sirius red staining

and showed elevated density of thickened collagen fibres in T2D ( $\approx 2$ -fold) that were significantly attenuated by both ANP and SACU treatments (by  $\approx 65\%$ ,  $\approx 50\%$ , and  $\approx 50\%$ , respectively; Figure 5J). Cardiac collagen was characterized using antibody arrays for Collagens I and III, along with Sircol assay for soluble collagen synthesis. In T2D, Collagen III increased by  $\approx 55\%$ , while soluble collagen decreased by  $\approx 40\%$ . ANP/SACU-treated groups exhibited opposite trends ( $\approx 30\%$  decrease in Collagen III,  $\approx 30\%$  increase in soluble collagen; Figure 5K–M). Finally, the increased SMAD3 but not SMAD2 activation in diabetic hearts was diminished by ANP/SACU treatments with  $\approx 65\%$  lower phosphorylation levels as compared with T2D (Figure 5N and O).



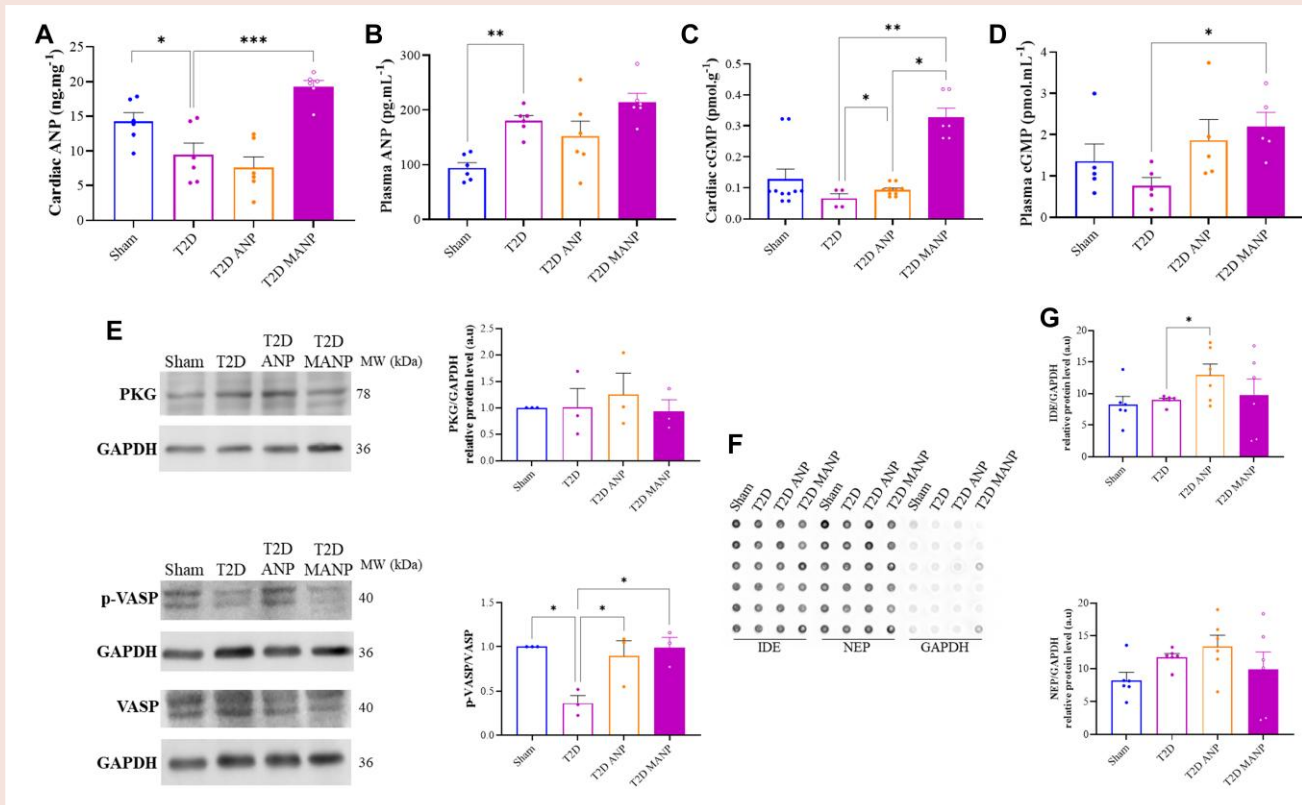


**Figure 4** High cardiac sustainability of M-atrial natriuretic peptide restores cardiac cyclic guanosine monophosphate/protein kinase G signalling in Type 2 diabetes. (A–D) Plasma and cardiac atrial natriuretic peptide and cyclic guanosine monophosphate concentrations measured by enzyme linked immunosorbent assay in the different rat groups. (E) Western blots and quantifications of cardiac protein kinase G, total and phosphorylated vasodilator-stimulated phosphoprotein in the different rat groups, with glyceraldehyde-3-phosphate dehydrogenase as an internal control. (F, G) Antibody arrays for insulin-degrading enzyme and neprilysin, using glyceraldehyde-3-phosphate dehydrogenase as internal control with respective quantifications for all groups. All quantitative data are reported as mean and individual data points  $\pm$  SEM. Normal distribution of the values was checked by the Shapiro–Wilk test and equal variance was checked by the Bartlett’s test. One-way analysis of variance followed by Sidak’s test in A, B, D, and E (lower panel), Kruskal–Wallis followed by Dunn’s test in C, and Brown–Forsythe and Welch analysis of variance followed by Dunnett’s T3 in E (upper panel) were performed. (A, B)  $n = 6$  animals for each group. (C)  $n = 5$  animals, each duplicate, for Sham and Type 2 diabetes atrial natriuretic peptide, and  $n = 4$ , 6 animals for Type 2 diabetes and Type 2 diabetes M-atrial natriuretic peptide. (D)  $n = 5$  animals for each group. (E)  $n = 3$  western blots from three animals for each group. \* $P < 0.05$ , and \*\* $P < 0.01$ . The figure was created with BioRender.com.

## Sacubitril attenuates cardiac extracellular signal-regulated kinases 1/2 and Jun amino-terminal kinases fibrotic signalling

Sacubitril treatment in combination with ANP modulated key fibrotic signalling pathways in T2D hearts. The antibody array analysis revealed that, while ERK1/2 and JNK were not significantly induced in T2D hearts, SACU/ANP still significantly reduced their activation as shown by the decrease of the phosphorylated/total protein levels compared with T2D controls, indicating a suppression of MAPK fibrotic signalling. Additionally, the level of ERK1/2 phosphorylation relative to GAPDH was decreased by SACU (Figure 6A and B).

## Sacubitril causes cardiac cyclic guanosine monophosphate accumulation in the myocardium of Type 2 diabetic rats

Similarly to the first set of experiments, cardiac ANP concentration decreased ( $\approx 50\%$ ) whereas plasma ANP increased ( $\approx 2$ -fold) in T2D vs.

Sham, with no noticeable effect for ANP treatment on both parameters (Figure 7A and B). Sacubitril single treatment or in combination with ANP increased cardiac but not plasma ANP levels ( $\approx 50\%$  vs. T2D) (Figure 7A and B). Additionally, cardiac and plasma cGMP levels were regarded as critical indicators for assessing peptide bioactivity. Cardiac cGMP levels fell (by 65%) in T2D but rose back to normal ( $\approx 1.5$ -fold vs. T2D) with ANP, SACU, or the combination. Nonetheless, neither the disease nor the various treatments had any effect on plasma cGMP levels (Figure 7C and D). Type 2 diabetes hindered the cardiac cGMP-dependent pathway PKG/VASP, as demonstrated by 60% lower VASP phosphorylation levels. Atrial natriuretic peptide, SACU, and the combination, on the other hand, activated this pathway, but the increase was only statistically significant with the latter ( $P = 0.17$ ,  $P = 0.16$ , and  $P < 0.05$ , respectively; Figure 7E). These results indicate that SACU and ANP similarly activate the cGMP signalling pathways in the myocardium of T2D rats. To further understand the non-cumulative effect of ANP/SACU combination on cGMP generation, we checked the cardiac expression levels of IDE and NEP. Insulin-degrading enzyme cardiac expression increased under ANP, SACU, and their combination, whereas NEP expression only increased under ANP/SACU (Figure 7F and G).



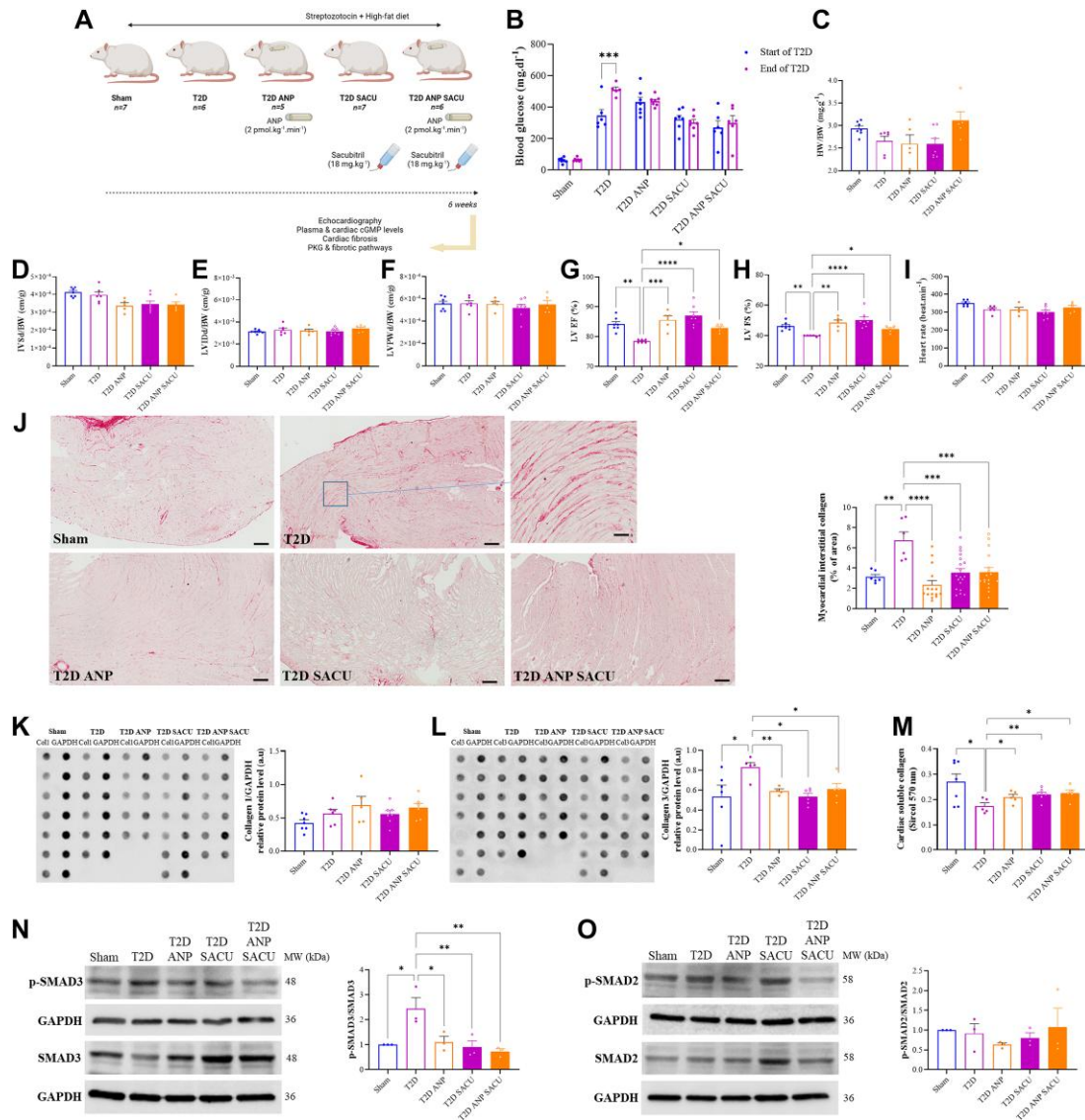


**Figure 5** Elevating natriuretic peptides alleviates Type 2 diabetes-induced myocardial fibrosis through the modulation of collagen turnover and SMADs signalling. (A) Streptozotocin injections and a high-fat diet were used to generate Type 2 diabetes in male rats. Atrial natriuretic peptide (2 pmol·kg<sup>-1</sup>·min<sup>-1</sup>) was delivered subcutaneously via osmotic pumps, and sacubitril (18 mg·kg<sup>-1</sup>·day<sup>-1</sup>) was provided orally. At 6 weeks, echocardiography examined cardiac function, followed by euthanasia for histological and molecular investigations of hearts and plasma. To account for differences in rat size, echocardiographic data were adjusted by dividing by body weight. (B) Blood glucose in Sham, Type 2 diabetes, Type 2 diabetes atrial natriuretic peptide, and Type 2 diabetes M-atrial natriuretic peptide. (C) Mean heart weight over body weight ratio. (D) Mean interventricular septum thickness at end-diastole. (E) Mean left ventricular internal dimension at end-diastole. (F) Mean left ventricular posterior wall thickness at end-diastole. (G) Mean left ventricular ejection fraction. (H) Mean left ventricular fractional shortening. (I) Heart rate in all groups. (J) Representative heart sections for all groups showing Sirius red staining with respective quantifications of analysed section areas. (K, L) Antibody arrays for cardiac Collagens I and III using glyceraldehyde-3-phosphate dehydrogenase as internal control with respective quantifications for all groups. (M) Cardiac soluble collagen for all groups using Sircol assay. (N, O) Representative western blots and densitometric analyses of phosphorylated and total SMAD2/3 (each with glyceraldehyde-3-phosphate dehydrogenase) for all groups. All quantitative data are reported as mean and individual data points ± SEM. Normal distribution of the values was checked by the Shapiro–Wilk test, and equal variance was checked by the Bartlett’s test. Repeated-measures two-way analysis of variance followed by Sidak’s test in B, one-way analysis of variance followed by Sidak’s test in D, E–G, I, and N or Holm–Sidak’s test in H, K, L, and O, and Kruskal–Wallis followed by Dunn’s test in C, J, and M were performed. (B–I) n = 5–7 animals according to each bar points, in B; one Type 2 diabetes has triplicate values. (J) n = 5–7 animals for each group, duplicate and triplicate values for Type 2 diabetes atrial natriuretic peptide, Type 2 diabetes sacubitril, and Type 2 diabetes atrial natriuretic peptide sacubitril from different heart region sections. (K–M) n = 5–7 animals according to each bar points. (N, O) n = 3 western blots from three animals for each group. \*P < 0.05, \*\*P < 0.01, \*\*\*P < 0.001, and \*\*\*\*P < 0.0001. ANP, atrial natriuretic peptide; GAPDH, glyceraldehyde-3-phosphate dehydrogenase; HW/BW, heart weight over body weight ratio; T2D, Type 2 diabetes; SACU, sacubitril. The figure was created with BioRender.com.

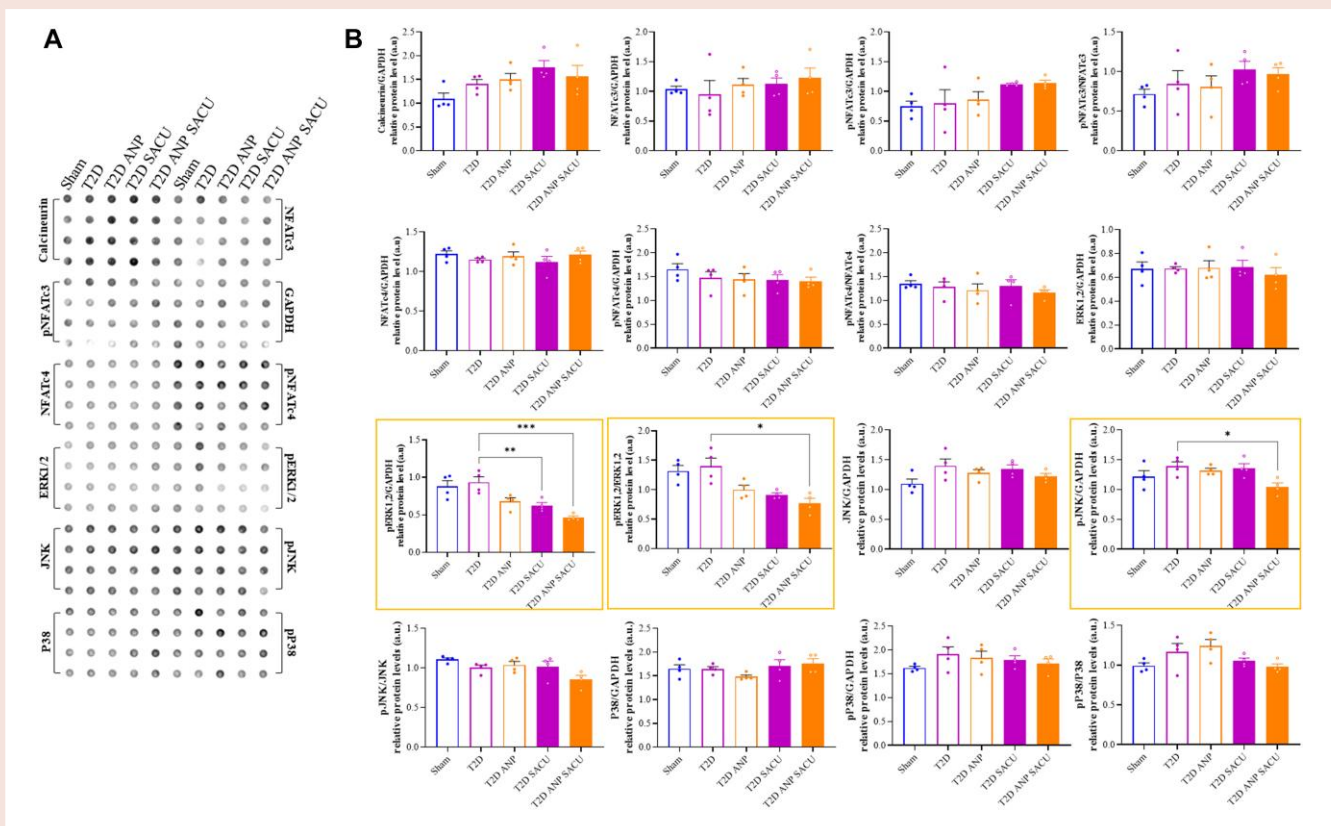


**Figure 6** Atrial natriuretic peptide and sacubitril inhibit cardiac atrial natriuretic peptide and Jun amino-terminal kinases fibrotic signalling in Type 2 diabetes. (A) Antibody arrays for calcineurin, nuclear factor of activated T cells 3, phospho-nuclear factor of activated T cells 3, nuclear factor of activated T cells 4, phospho-nuclear factor of activated T cells 4, extracellular signal-regulated kinases 1/2, phospho-extracellular signal-regulated kinases 1/2, Jun amino-terminal kinases, phospho-Jun amino-terminal kinases, P38, and phospho-P38, using glyceraldehyde-3-phosphate dehydrogenase as internal control with respective quantifications (B) for all groups. All quantitative data are reported as mean and individual data points  $\pm$  SEM. Normal distribution of the values was checked by the Shapiro–Wilk test, and equal variance was checked by the Bartlett’s test. One-way analysis of variance followed by Sidak’s tests was performed.  $n = 4$  animals according to each bar point ( $n = 1$  array for each protein set). \* $P < 0.05$ , \*\* $P < 0.01$ , and \*\*\* $P < 0.001$ . ANP, atrial natriuretic peptide; ERK1/2, extracellular signal-regulated kinases 1/2; GAPDH, glyceraldehyde-3-phosphate dehydrogenase; NFATc3, nuclear factor of activated T cells 3; NFATc4, nuclear factor of activated T cells 4; SACU, sacubitril; T2D, Type 2 diabetes. The figure was created with BioRender.com.

## Discussion

The main finding of the present study is that myocardial bioavailability of ANP is a major determinant of peptide efficacy in reducing cardiac fibrosis and improving pump function during diabetic cardiomyopathy. We found a balance between peptide elimination and activation of cGMP-dependent signalling pathways that plays a crucial role in the antifibrotic effects of ANP on myocardium. Furthermore, our results indicate that reducing myocardial fibrosis is a major therapeutic target of heart failure that can be reached by modulating NP half-life.<sup>30–32</sup>

Among diabetic experimental models, STZ-induced diabetes reliably replicates diabetes-related features and complications in humans<sup>33</sup> notably prominent myocardial fibrosis.<sup>21–26</sup> Furthermore, in the literature, an antifibrotic effect of NP has been reported during heart failure.<sup>30–32,34</sup> Besides, other studies have described a local function of the ANP/GC-A system in moderating the molecular program of cardiac hypertrophy.<sup>35</sup> In this regard, the enhanced antifibrotic effect of the mutated vs. wild-type ANP could account for the former’s superior efficacy in ameliorating cardiac function of STZ-diabetic rats. Cardiac fibrosis is characterized by collagen turnover and phenotype switch leading to increased myocardial stiffness.<sup>36</sup> Herein, we found an important

decrease in collagen Type III in the diabetic hearts under MANP along an increase in the soluble collagen. This collagen phenotype fine-tuning might play a crucial role in preserving cardiac performance of the fibrotic heart. In the early stages of heart failure, collagen Type III replaces collagen Type I leading to cardiomyocyte slippage and fibrotic extracellular matrix. Therefore, the breakdown of collagen Type I and the buildup of poorly cross-linked collagen Type III are crucial for myocardial fibrosis and ventricular remodelling.<sup>37</sup> At the molecular level, ANP and transforming growth factor- $\beta$  (TGF- $\beta$ ) are known to play counter-regulatory roles in cardiovascular physiology and disease. TGF- $\beta$  acts via its downstream SMAD proteins to mediate fibroblast proliferation, differentiation and collagen deposition, whereas ANP acts as an inhibitor of this pathway.<sup>28,38</sup> Moreover, collagen assembly is subtly regulated by several structural proteins, in particular secreted protein acidic and rich in cysteine, that seems to be up-regulated in the diabetic heart,<sup>39,40</sup> stimulated by TGF- $\beta$ ,<sup>41</sup> and thus might be inhibited by ANP. Further molecular analysis showed an intricate fine-tuning of non-canonical TGF- $\beta$  fibrotic pathways, calcineurin/NFAT and MAPK, where MANP exerted regulatory control even in the absence of overt activation in T2D. The calcineurin/NFAT and MAPK signalling pathways, including ERK1/2, promote cardiac fibrosis by driving fibroblast proliferation,

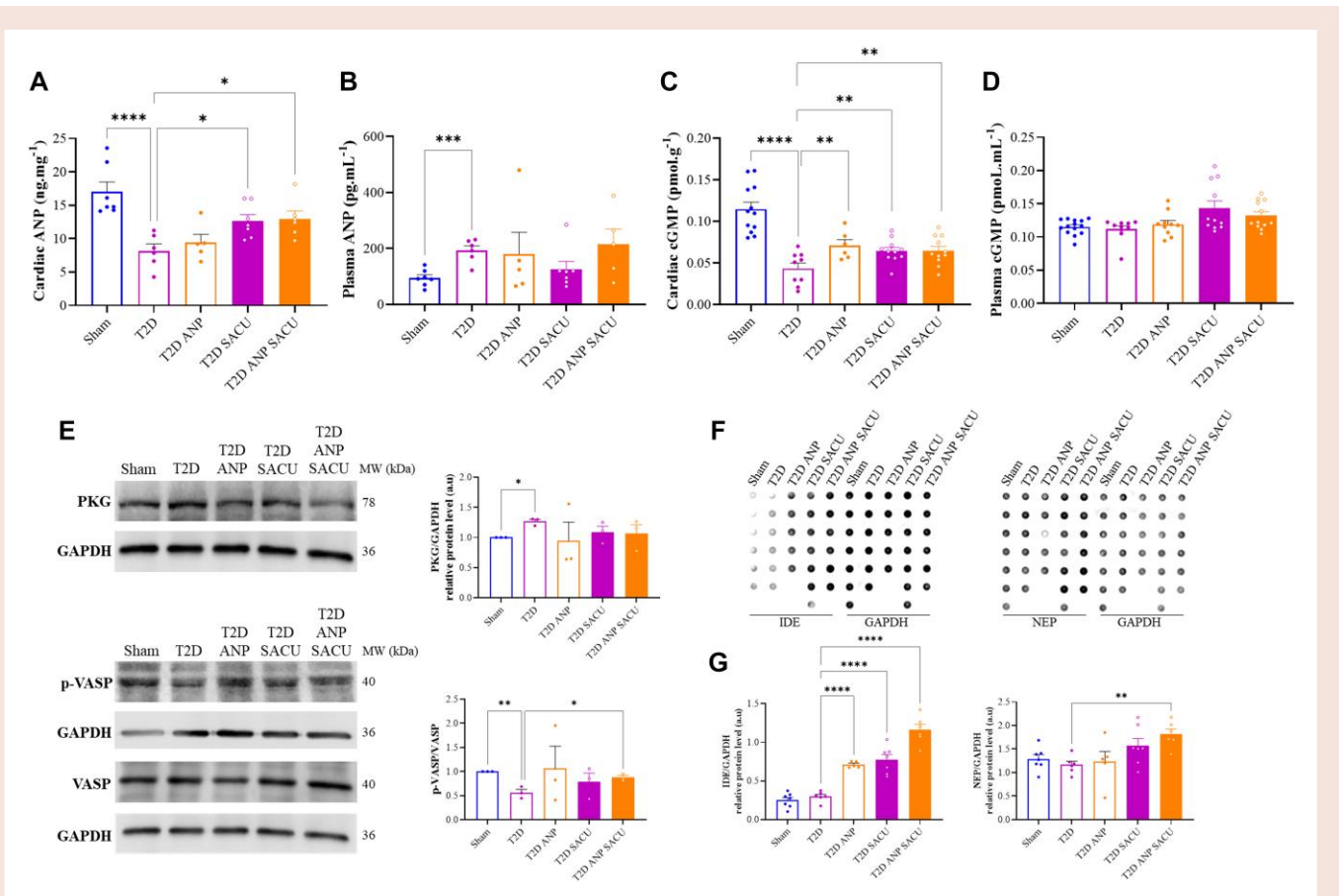


**Figure 7** Impact of atrial natriuretic peptide-enhancing strategies on cardiac cyclic guanosine monophosphate levels. (A–D) Plasma and cardiac atrial natriuretic peptide and cyclic guanosine monophosphate concentrations measured by enzyme linked immunosorbent assay in the different rat groups. (E) Western blots and quantifications of cardiac protein kinase G, total, and phosphorylated vasodilator-stimulated phosphoprotein in the different rat groups, with glyceraldehyde-3-phosphate dehydrogenase as an internal control. (F, G) Antibody arrays for insulin-degrading enzyme and neprilysin, using glyceraldehyde-3-phosphate dehydrogenase as internal control with respective quantifications for all groups. All quantitative data are reported as mean and individual data points  $\pm$  SEM. Normal distribution of the values was checked by the Shapiro–Wilk test, and equal variance was checked by the Bartlett’s test. One-way analysis of variance followed by Sidak’s test in A–C, Kruskal–Wallis followed by Dunn’s test in D, and Brown–Forsythe and Welch analysis of variance followed by Dunnett’s T3 in E were performed. (A, B)  $n = 5–7$  animals for each group. (C, D)  $n = 5–7$  animals for each group, each in duplicate. (E)  $n = 3$  western blots from three animals for each group. \* $P < 0.05$ , \*\* $P < 0.01$ , \*\*\* $P < 0.001$ , and \*\*\*\* $P < 0.0001$ . ANP, atrial natriuretic peptide; ERK1/2, extracellular signal-regulated kinases 1/2; GAPDH, glyceraldehyde-3-phosphate dehydrogenase; MANP, M-atrial natriuretic peptide; NFATc3, nuclear factor of activated T cells 3; NFATc4, nuclear factor of activated T cells 4; PKG, protein kinase G; T2D, Type 2 diabetes; VASP, vasodilator-stimulated phosphoprotein. The figure was created with BioRender.com.

myofibroblast differentiation, and extracellular matrix deposition, contributing to maladaptive cardiac remodeling.<sup>42–44</sup> The inhibition of NFATc3 and ERK1/2 highlights MANP’s ability to modulate profibrotic responses, and these findings align with the previous results strengthening the antifibrotic effects of MANP.

Cardiac fibroblasts are the key cellular players in myocardial fibrosis through their high potential to migrate, proliferate, and trans-differentiate into myofibroblasts that synthesize extracellular matrix components.<sup>45,46</sup> Several markers have been used to study cardiac fibroblast population in the normal and diseased hearts.<sup>47,48</sup> Our findings show that both wild-type and MANP similarly inhibit fibroblast activation *in vitro* as evidenced by the reduced collagen production and proliferation. We previously reported that the NPs regulate fibroblast activation through the ANP/GC-A/cGMP signalling cascades.<sup>49</sup> Interestingly, both wild-type and MANP show comparable effects on intracellular cGMP accumulation, cell proliferation, collagen secretion,

and SMAD activation, indicating that the two peptide isoforms share the same affinity for NPR-A and NPR-C clearance receptors as reported in the literature.<sup>13,14</sup> Therefore, *in vitro* data cannot explain the difference observed *in vivo* between wild-type and mutated peptides on myocardial fibrosis and the up-regulation of TGF- $\beta$  SMAD-dependent pathway.<sup>50</sup> The explanation is most likely due to reduced clearance of the mutated peptide responsible for enhanced ANP and cGMP myocardial concentrations together with the up-regulation of the cGMP-dependent PKG signalling pathway in MANP- vs. ANP-treated STZ-diabetic rats.<sup>13,14</sup> The slight increase in plasma cGMP in MANP-treated animals might also result from low peripheral peptide degradation. In T2D, the decrease in cardiac ANP and cGMP, despite increased plasma ANP and stable plasma cGMP, suggests impaired myocardial ANP retention and signalling. This may result from increased cardiac ANP degradation via NEP or the up-regulated IDE demonstrated by our antibody array, reduced NPR-A receptor



function, or enhanced NPR-C-mediated clearance.<sup>38</sup> Additionally, diminished cardiac ANP effects due to increased phosphodiesterase activity could further suppress cGMP accumulation,<sup>51,52</sup> despite sufficient circulating ANP.<sup>53</sup> The stable plasma cGMP levels indicate preserved systemic NP signalling, due to the other numerous non-cardiac sources of cGMP secretion, but the disrupted cardiac response further highlights the importance of local regulation.

To test the involvement of the coupling between ANP degradation and activation of cGMP-dependent signalling pathway, STZ-diabetic rats were treated with the NEP inhibitor SACU. Indeed, SACU treatment demonstrated similar efficiency to ANP in improving cardiac performance, reducing myocardial fibrosis, and inhibiting the SMAD profibrotic signalling pathway. Similarly to MANP, SACU, either alone or in combination with ANP, demonstrated fine-tuning of important fibrotic signalling pathways in the heart, particularly in the MAPK cascade, including ERK1/2 and JNK. Like ERK1/2, JNK plays a critical role in driving myocardial fibrosis.<sup>44</sup> Still, further exploration of other cGMP/PKG targets, such as ion channels and pumps, would provide additional insight into cGMP/PKG's role in mediating SACU/MANP's effects in the diabetic heart. Furthermore, SACU, like ANP, increased myocardial ANP and cGMP accumulation and up-regulated cGMP-dependent PKG signalling. These findings are consistent with SACU's ability to reduce biomarkers of profibrotic signalling in heart failure.<sup>54</sup> Of note, SACU, contrary to MANP, was not superior to ANP in terms of fibrosis reduction and cardiac function improvement and did not exhibit additional benefits when combined with ANP. This might be due to the compensatory clearance pathways, due to NEP inhibition, such as IDE, as demonstrated by our antibody array analysis, other endopeptidases or the NPR-C clearance receptor.<sup>3</sup> In fact, NPR-C deletion inhibits TGF- $\beta$  pathway in cardiac fibroblasts leading to reduced myocardial fibrosis.<sup>38</sup> Besides, this local NP control system is crucial in maintaining ANP levels within the myocardium. When ANP is administered in conditions where NEP is overexpressed in the heart, cGMP levels increase in the plasma but not in the cardiac tissue, resulting in a lack of cardioprotective effects.<sup>55</sup> Still, the expression and activation pattern of ANP receptors as well as endopeptidase activity remain poorly investigated overall in diabetic cardiomyopathy and heart disease.<sup>38,56,57</sup> Of note, MANP, ANP, SACU, and their combination reduced urine output, water intake, and food intake in T2D animals without affecting the body weight (see [Supplementary material online, Figures S1 and S2](#)), indicating an improvement in diabetes hallmarks consistent with reduced blood glucose levels. The body weight of T2D rats remained unchanged, aligning with existing literature that indicates obesity in rats typically develops over extended periods (>3 months). A notable increase in body weight is usually observed following high-fat diet, which subsequently declines after STZ administration.<sup>58,59</sup> Natriuretic peptides have increasingly been shown to play a role in metabolism, influencing multiple metabolic pathways.<sup>60,61</sup> While the peptide dose used herein does not significantly impact haemodynamics, it may slightly affect diuresis as previously described.<sup>15</sup> However, the potential diuretic effects of MANP, ANP, and SACU might have been masked by diabetes amelioration. Furthermore, in the referenced study, plasma ANP and cGMP increased ~1.5-fold in mongrel dogs following ANP or MANP administration. In contrast, our study found no significant change in plasma ANP or cGMP levels in diabetic rats treated with ANP or MANP, despite prolonged exposure via osmotic pumps. These systemic metabolic improvements could indirectly contribute to improved cardiac outcomes, as hyperglycaemia is known to exacerbate myocardial fibrosis and dysfunction, yet the different treatments produced relatively comparable systemic metabolic effects. Thus, while systemic improvements could modulate the disease environment, they do not fully explain the observed cardiac effects. Our findings reinforce the critical role of myocardial ANP/cGMP accumulation, highlighting that systemic ANP levels alone are insufficient to drive cardioprotection unless the local cardiac regulatory mechanisms are optimized.

In view of these multifactorial complexities, more research is required to dissect the pathways underlying the antifibrotic effect of MANP along with ANP. Nevertheless, these results support our central hypothesis on the myocardial bioavailability of ANP as a key determinant of its efficacy in reducing fibrosis and improving cardiac function. The differential accumulation of ANP and cGMP in cardiac tissue, rather than systemic circulation, strongly indicates that local rather than systemic mechanisms drive the beneficial effects observed. Given that cGMP pathway is compromised in patients with heart failure,<sup>4,5,62</sup> cGMP-enhancing therapies are increasingly showing promising clinical outcomes.<sup>63,64</sup>

## Limitations

This study presents certain limitations. For a more comprehensive evaluation of MANP's effects on cardiac fibrosis, longer-term studies should be conducted at advanced stages of heart failure as well as on survival outcomes to better mimic the long-term progression of diabetic cardiomyopathy in humans. Additionally, exploring a range of MANP dosages could provide valuable insights into its safety and effectiveness. While our results demonstrate MANP's substantial effect on cardiac fibrosis, potential haemodynamic and systemic effects (natriuresis, blood pressure, effect on insulin secretion, and peripheral insulin sensitivity) of ANP and MANP guarantee further exploration. The study assessed the preventive effects of MANP/ANP administered at the time of diabetes induction; since this does not fully reflect the clinical settings where treatment typically begins after disease establishment, additional studies are required whereby ANP is tested in pre-established diabetes. Furthermore, the studied treatments could be combined to other established ones for diabetes and heart disease such as sodium-glucose transporter 2 inhibitors, since these combination therapies are increasingly showing positive outcomes.<sup>65–68</sup>

## Conclusions

The ANP antifibrotic cardiac effect is related to its myocardial bioavailability, which is determined by the rate of peptide degradation. The efficacy of MANP in improving cardiac performance in diabetes appears to be primarily related to its myocardial accumulation and activation of cGMP-dependent PKG signalling pathways. Enhancing ANP tissue accumulation could be an important and promising therapeutic strategy in the management of fibrosis in heart failure.

## Lead author biography



Jules J. Bakhos, a graduate of the Faculty of Medicine of the Saint Joseph University of Beirut, holds a MD and a Research MSc degree in Physiology and Pathophysiology. Physician-researcher at the Cleveland Clinic, he specializes in preventive cardiology, public health, and medical innovation. His work focuses on cardiovascular disease prevention, health policy, and tobacco control. As the founder of NAFAS, a smoking cessation non-profit, and a medical social media platform, he leads initiatives

in health promotion and public health advocacy. Dr Bakhos has contributed to multiple peer-reviewed publications and collaborates on research advancing evidence-based strategies to improve patient outcomes.



Youakim Saliba, an associate professor at Saint-Joseph University of Beirut's Faculty of Medicine, holds a PhD in Physiology and Pathophysiology from Sorbonne Université and Saint-Joseph University. An integral member of the Laboratory of Research in Physiology and Pathophysiology, he engages in cutting-edge research on cardiac and renal fibrosis, with numerous publications in high-impact journals, while providing mentorship to medical students. He is an academic editor for Cardiovascular

Therapeutics and a reviewer for multiple scientific journals. His contributions have been recognized with eminent international awards from the International Union of Physiological Sciences, the Federation of European Physiological Societies, and France Excellence Eiffel.



Stéphane N. Hatem is an MD in cardiovascular diseases and PhD in cardiac physiology. He is a full professor of cardiovascular physiology (Sorbonne Université and Paris Hospital, APHP). Since 2019, he is a director of the University-Hospital institutes the IHU-ICAN dedicated to research and care on cardiometabolic diseases. He has been the European coordinator of a Leducq TransAtlantic Network (2009–14) and partner in two European (FP7 EUTRAF and H2020

CATCHE ME) networks. He is the coordinator of the H2020 MAESTRIA consortium. His research activity has been entirely dedicated to deciphering the pathophysiology of atrial fibrillation notably the role played by natriuretic peptides and by epicardial adipose tissue. His research has contributed to the concept of the atrial cardiomyopathy.



Nassim Fares is a full professor of Physiology at the Faculty of Medicine, Saint-Joseph University of Beirut, founder and head of the Research Laboratory of Physiology and Pathophysiology. His laboratory is an international associated laboratory of UMR51166-ICAN, Pitié-Salpêtrière, France. A former graduate of the prestigious Electrophysiology School of Poitiers, France, he has strong expertise in cardiovascular physiology. His research focuses on cardiovascular diseases, particularly the mechanisms underlying cardiac and renal fibrosis. His team works to unravel the cellular and molecular processes driving fibrogenesis and identify innovative therapeutic strategies. His contributions earned recognition through French–Lebanese intergovernmental awards, including CNRS-L and CEDRE.

His team works to unravel the cellular and molecular processes driving fibrogenesis and identify innovative therapeutic strategies. His contributions earned recognition through French–Lebanese intergovernmental awards, including CNRS-L and CEDRE.

## Data availability

The data that support the findings of this study are available from the corresponding authors upon reasonable request.

## Supplementary material

Supplementary material is available at *European Heart Journal Open* online.

## Ethical approval

The present research was approved by Saint Joseph University of Beirut's Ethics Committee (Project #FM348, mixed project USJ/CNRS-L). The protocols used were developed in accordance with the American Physiological Society Council's Guiding Principles in the Care and Use of Animals, the US National Institutes of Health's Guide for the Care and Use of Laboratory Animals (NIH publication no. 85-23, revised 1985), and the European Parliament Directive 2010/63 EU. The animals were housed in a controlled specific pathogen-free environment in individually ventilated cages with hygienic bedding from crushed beech wood (EAN5410340230947; Versele-Laga, Deinze, Belgium) and were exposed to a constant temperature of 25°C and humidity level of 50 ± 5% and a 12:12-h light/dark cycle. A maximum of three rats were housed per cage. They were given regular rodent food (EAN5410340615096; Versele-Laga, Deinze, Belgium) containing protein 20%, fat content 3.5%, crude fibre 4%, crude ash 7%, calcium 1.1%, and phosphorus 0.75%, with unfettered access to tap water. They were given at least 1 week to adjust to these conditions before the inquiry began. No mortality was observed in the two sets of experiments. Sample sizes have been clarified in Methods section and each of the figure legends. Additionally, for certain parameters such as echocardiography and immunofluorescence for the first set, not all animals were used due to technical constraints, including limited anaesthesia and antibody availability. Cardiac cGMP and Sirius red analyses included duplicates from different heart regions to ensure comprehensive evaluation while utilizing all animals in each group. All raw data have been presented transparently in the study.

## Funding

This work was jointly funded by the Research Council of The Saint-Joseph University of Beirut (grant #FM348), the Conseil National de la Recherche Scientifique-Liban (CNRS-L) Grant Research Program (GRP 2019), and Partenariat Hubert Curien franco-libanais (PHC CEDRE) PROJECT N° 4782VA.

**Conflict of interest:** None declared.

## References

1. Kuwahara K. The natriuretic peptide system in heart failure: diagnostic and therapeutic implications. *Pharmacol Ther* 2021;**227**:107863.
2. Numata G, Takimoto E. Cyclic GMP and PKG signaling in heart failure. *Front Pharmacol* 2022;**13**:792798.
3. Potter LR. Natriuretic peptide metabolism, clearance and degradation. *FEBS J* 2011;**278**:1808–1817.
4. Subramanya V, Zhao D, Ouyang P, Ying W, Vaidya D, Ndumele CE, Lima JA, Guallar E, Hoogeveen RC, Shah SJ, Heckbert SR, Kass DA, Post WS, Michos ED. Cyclic guanosine monophosphate and 10-year change in left ventricular mass: the Multi-Ethnic Study of Atherosclerosis (MESA). *Biomarkers* 2021;**26**:309–317.
5. Ying W, Zhao D, Ouyang P, Subramanya V, Vaidya D, Ndumele CE, Guallar E, Sharma K, Shah SJ, Kass DA, Hoogeveen RC, Lima JA, Heckbert SR, deFilippi CR, Post WS, Michos ED. Associations between the cyclic guanosine monophosphate pathway and cardiovascular risk factors: MESA. *J Am Heart Assoc* 2019;**8**:e013149.
6. Nogi K, Ueda T, Matsue Y, Nogi M, Ishihara S, Nakada Y, Kawakami R, Kagiya N, Kitai T, Oishi S, Akiyama E, Suzuki S, Yamamoto M, Kida K, Okumura T, Saito Y. Effect of carperitide on the 1 year prognosis of patients with acute decompensated heart failure. *ESC Heart Fail* 2022;**9**:1061–1070.
7. McMurray JJV, Packer M, Desai AS, Gong J, Lefkowitz MP, Rizkala AR, Rouleau JL, Shi VC, Solomon SD, Swedberg K, Zile MR; PARADIGM-HF Investigators and Committees. Angiotensin–neprilysin inhibition versus enalapril in heart failure. *N Engl J Med* 2014;**371**:993–1004.
8. Pfeffer MA, Claggett B, Lewis EF, Granger CB, Køber L, Maggioni AP, Mann DL, McMurray JJV, Rouleau J-L, Solomon SD, Steg PG, Berwanger O, Cikes M, De Pasquale CG, East C, Fernandez A, Jering K, Landmesser U, Mehran R, Merkely B, Vaghaniwalla Mody F, Petrie MC, Petrov I, Schou M, Senni M, Sim D, van der Meer P, Lefkowitz M, Zhou Y, Gong J, Braunwald E; PARADISE-MI Investigators and Committees. Angiotensin receptor–neprilysin inhibition in acute myocardial infarction. *N Engl J Med* 2021;**385**:1845–1855.

9. Solomon SD, McMurray JJV, Anand IS, Ge J, Lam CSP, Maggioni AP, Martinez F, Packer M, Pfeffer MA, Pieske B, Redfield MM, Rouleau JL, van Veldhuisen DJ, Zannad F, Zile MR, Desai AS, Claggett B, Jhund PS, Boytsov SA, Comin-Colet J, Cleland J, Dünken H-D, Gonçalvesova E, Katova T, Kerr Saraiva JF, Lelonek M, Merkely B, Senni M, Shah SJ, Zhou J, Rizkala AR, Gong J, Shi VC, Lefkowitz MP; PARAGON-HF Investigators and Committees. Angiotensin-neprilysin inhibition in heart failure with preserved ejection fraction. *N Engl J Med* 2019;**381**:1609–1620.
10. Velazquez EJ, Morrow DA, DeVore AD, Duffy CI, Ambrosy AP, McCague K, Rocha R, Braunwald E; PIONEER-HF Investigators. Angiotensin-neprilysin inhibition in acute decompensated heart failure. *N Engl J Med* 2019;**380**:539–548.
11. Bozkurt B, Nair AP, Misra A, Scott CZ, Mahar JH, Fedson S. Neprilysin inhibitors in heart failure: the science, mechanism of action, clinical studies, and unanswered questions. *JACC Basic Transl Sci* 2023;**8**:88–105.
12. Ibrahim NE, McCarthy CP, Shrestha S, Gaggin HK, Mukai R, Szymonifka J, Apple FS, Burnett JC, Iyer S, Januzzi JL. Effect of neprilysin inhibition on various natriuretic peptide assays. *J Am Coll Cardiol* 2019;**73**:1273–1284.
13. Dickey DM, Yoder AR, Potter LR. A familial mutation renders atrial natriuretic peptide resistant to proteolytic degradation. *J Biol Chem* 2009;**284**:19196–19202.
14. Ralat LA, Guo Q, Ren M, Funke T, Dickey DM, Potter LR, Tang W-J. Insulin-degrading enzyme modulates the natriuretic peptide-mediated signaling response. *J Biol Chem* 2011;**286**:4670–4679.
15. McKie PM, Cataliotti A, Huntley BK, Martin FL, Olson TM, Burnett JC. A human atrial natriuretic peptide gene mutation reveals a novel peptide with enhanced blood pressure-lowering, renal-enhancing, and aldosterone-suppressing actions. *J Am Coll Cardiol* 2009;**54**:1024–1032.
16. McKie PM, Cataliotti A, Boerrigter G, Chen HH, Sangaralingham SJ, Martin FL, Ichiki T, Burnett JC. A novel atrial natriuretic peptide based therapeutic in experimental angiotensin II mediated acute hypertension. *Hypertension* 2010;**56**:1152–1159.
17. Dzhozashvili NA, Iyer SR, Chen HH, Burnett JC. MANP (M-atrial natriuretic peptide) reduces blood pressure and furosemide-induced increase in aldosterone in hypertension. *Hypertension* 2022;**79**:750–760.
18. Chen Y, Schaefer JJ, Iyer SR, Harders GE, Pan S, Sangaralingham SJ, Chen HH, Redfield MM, Burnett JC. Long-term blood pressure lowering and cGMP-activating actions of the novel ANP analog MANP. *Am J Physiol Regul Integr Comp Physiol* 2020;**318**:R669–R676.
19. Chen HH, Wan S-H, Iyer SR, Cannone V, Sangaralingham SJ, Nuetel J, Burnett JC. First-in-human study of MANP: a novel ANP (atrial natriuretic peptide) analog in human hypertension. *Hypertension* 2021;**78**:1859–1867.
20. McKie PM, Cataliotti A, Ichiki T, Sangaralingham SJ, Chen HH, Burnett JC. M-atrial natriuretic peptide and nitroglycerin in a canine model of experimental acute hypertensive heart failure: differential actions of 2 cGMP activating therapeutics. *J Am Heart Assoc* 2014;**3**:e000206.
21. Patel KV, Segar MW, Klonoff DC, Khan MS, Usman MS, Lam CSP, Verma S, DeFilippis AP, Nasir K, Bakker SJL, Westenbrink BD, Dullaart RPF, Butler J, Vaduganathan M, Pandey A. Optimal screening for predicting and preventing the risk of heart failure among adults with diabetes without atherosclerotic cardiovascular disease: a pooled cohort analysis. *Circulation* 2024;**149**:293–304.
22. Su Q, Huang W, Huang Y, Dai R, Chang C, Li Q-Y, Liu H, Li Z, Zhao Y, Wu Q, Pan D-G. Single-cell insights: pioneering an integrated atlas of chromatin accessibility and transcriptomic landscapes in diabetic cardiomyopathy. *Cardiovasc Diabetol* 2024;**23**:139.
23. Li W, Lou X, Zha Y, Qin Y, Hong L, Xie Z, Yang S, Wang C, An J, Zhang Z, Qiao S. Single-cell RNA-seq of heart reveals intercellular communication drivers of myocardial fibrosis in diabetic cardiomyopathy. *eLife* 2023;**12**:e80479.
24. Cheng Y, Wang Y, Yin R, Xu Y, Zhang L, Zhang Y, Yang L, Zhao D. Central role of cardiac fibroblasts in myocardial fibrosis of diabetic cardiomyopathy. *Front Endocrinol (Lausanne)* 2023;**14**:1162754.
25. Pua CJ, Loo G, Kui M, Moy WL, Hii A-A, Lee V, Chin C-T, Bryant JA, Toh D-F, Lee C-H, Cook SA, Richards AM, Le T-T, Chin CWL. Impact of diabetes on myocardial fibrosis in patients with hypertension: the REMODEL study. *Circ Cardiovasc Imaging* 2023;**16**:545–553.
26. Pan K-L, Hsu Y-C, Chang S-T, Chung C-M, Lin C-L. The role of cardiac fibrosis in diabetic cardiomyopathy: from pathophysiology to clinical diagnostic tools. *Int J Mol Sci* 2023;**24**:8604.
27. Rahmutula D, Zhang H, Wilson EE, Olgin JE. Absence of natriuretic peptide clearance receptor attenuates TGF- $\beta$ 1-induced selective atrial fibrosis and atrial fibrillation. *Cardiovasc Res* 2019;**115**:357–372.
28. Li P, Wang D, Lucas J, Oparil S, Xing D, Cao X, Novak L, Renfrow MB, Chen Y-F. Atrial natriuretic peptide inhibits transforming growth factor beta-induced Smad signaling and myofibroblast transformation in mouse cardiac fibroblasts. *Circ Res* 2008;**102**:185–192.
29. Bubikat A, De Windt LJ, Zetsche B, Fabritz L, Sickler H, Eckardt D, Gödecke A, Baba HA, Kuhn M. Local atrial natriuretic peptide signaling prevents hypertensive cardiac hypertrophy in endothelial nitric-oxide synthase-deficient mice. *J Biol Chem* 2005;**280**:21594–21599.
30. Han M, Liu Z, Liu L, Huang X, Wang H, Pu W, Wang E, Liu X, Li Y, He L, Li X, Wu J, Qiu L, Shen R, Wang Q-D, Ji Y, Ardehali R, Shu Q, Lui KO, Wang L, Zhou B. Dual genetic tracing reveals a unique fibroblast subpopulation modulating cardiac fibrosis. *Nat Genet* 2023;**55**:665–678.
31. Frangogiannis NG. Cardiac fibrosis. *Cardiovasc Res* 2021;**117**:1450–1488.
32. Gyöngyösi M, Winkler J, Ramos I, Do Q-T, Firat H, McDonald K, González A, Thum T, Diez J, Jaisser F, Pizard A, Zannad F. Myocardial fibrosis: biomedical research from bench to bedside. *Eur J Heart Fail* 2017;**19**:177–191.
33. Jasińska-Stroschein M. The current state of preclinical modeling of human diabetic cardiomyopathy using rodents. *Biomed Pharmacother* 2023;**168**:115843.
34. Tamura N, Ogawa Y, Chusho H, Nakamura K, Nakao K, Suda M, Kasahara M, Hashimoto R, Katsuura G, Mukoyama M, Itoh H, Saito Y, Tanaka I, Otani H, Katsuki M. Cardiac fibrosis in mice lacking brain natriuretic peptide. *Proc Natl Acad Sci U S A* 2000;**97**:4239–4244.
35. Molkentin JD. A friend within the heart: natriuretic peptide receptor signaling. *J Clin Invest* 2003;**111**:1275–1277.
36. Nikolov A, Popovski N. Extracellular matrix in heart disease: focus on circulating collagen Type I and III derived peptides as biomarkers of myocardial fibrosis and their potential in the prognosis of heart failure: a concise review. *Metabolites* 2022;**12**:297.
37. Sofia C, Georgiadou P, Sbarouni E, Voudris V. Chronic heart failure and serum collagen. In: Preedy VR and Patel VB, eds. *General Methods in Biomarker Research and Their Applications*. Dordrecht: Springer Netherlands; 2015. p689–707.
38. Meng L, Lu Y, Wang X, Cheng C, Xue F, Xie L, Zhang Y, Sui W, Zhang M, Zhang Y, Zhang C. NPRC deletion attenuates cardiac fibrosis in diabetic mice by activating PKA/PKG and inhibiting TGF- $\beta$ 1/Smad pathways. *Sci Adv* 2023;**9**:eadd4222.
39. Kos K, Wilding JPH. SPARC: a key player in the pathologies associated with obesity and diabetes. *Nat Rev Endocrinol* 2010;**6**:225–235.
40. McCurdy S, Baicu CF, Heymans S, Bradshaw AD. Cardiac extracellular matrix remodeling: fibrillar collagens and secreted protein acidic and rich in cysteine (SPARC). *J Mol Cell Cardiol* 2010;**48**:544–549.
41. Engebretsen KVT, Skårdal K, Bjørnstad S, Marstein HS, Skrbic B, Sjaastad I, Christensen G, Bjørnstad JL, Tønnessen T. Attenuated development of cardiac fibrosis in left ventricular pressure overload by SM16, an orally active inhibitor of ALK5. *J Mol Cell Cardiol* 2014;**76**:148–157.
42. Olson ER, Shamhart PE, Naugle JE, Meszaros JG. Angiotensin II-induced extracellular signal-regulated kinase 1/2 activation is mediated by protein kinase Cdelta and intracellular calcium in adult rat cardiac fibroblasts. *Hypertension* 2008;**51**:704–711.
43. Saliba Y, Jebara V, Hajal J, Maroun R, Chacar S, Smayra V, Abramowitz J, Birnbaumer L, Farès N. Transient receptor potential canonical 3 and nuclear factor of activated T cells C3 signaling pathway critically regulates myocardial fibrosis. *Antioxid Redox Signal* 2019;**30**:1851–1879.
44. Zhang Z, Yang Z, Wang S, Wang X, Mao J. Targeting MAPK-ERK/JNK pathway: a potential intervention mechanism of myocardial fibrosis in heart failure. *Biomed Pharmacother* 2024;**173**:116413.
45. Kuwabara JT, Hara A, Bhutata S, Gojanovich GS, Chen J, Hokutan K, Shettigar V, Lee AY, DeAngelo LP, Heckl JR, Jahansooz JR, Tacold DK, Ziolo MT, Apte SS, Tallquist MD. Consequences of PDGFR $\alpha$  fibroblast reduction in adult murine hearts. *eLife* 2022;**11**:e69854.
46. Kanisicak O, Khalil H, Ivey MJ, Karch J, Maliken BD, Correll RN, Brody MJ, Lin S-C, Aronow BJ, Tallquist MD, Molkentin JD. Genetic lineage tracing defines myofibroblast origin and function in the injured heart. *Nat Commun* 2016;**7**:12260.
47. Pinto AR, Illykh A, Ivey MJ, Kuwabara JT, D'Antoni ML, Debuque R, Chandran A, Wang L, Arora K, Rosenthal NA, Tallquist MD. Revisiting cardiac cellular composition. *Circ Res* 2016;**118**:400–409.
48. Moore-Morris T, Guimarães-Camboa N, Banerjee I, Zambon AC, Kisseleva T, Velayoudon A, Stallcup WB, Gu Y, Dalton ND, Cedenilla M, Gomez-Amaro R, Zhou B, Brenner DA, Peterson KL, Chen J, Evans SM. Resident fibroblast lineages mediate pressure overload-induced cardiac fibrosis. *J Clin Invest* 2014;**124**:2921–2934.
49. Moubarak M, Magaud C, Saliba Y, Chatelier A, Bois P, Fèvre J-F, Fares N. Effects of atrial natriuretic peptide on rat ventricular fibroblasts during differentiation into myofibroblasts. *Physiol Res* 2015;**64**:495–503.
50. Hanna A, Humeres C, Frangogiannis NG. The role of Smad signaling cascades in cardiac fibrosis. *Cell Signal* 2021;**77**:109826.
51. Mátyás C, Németh BT, Oláh A, Hidi L, Birtalan E, Kellermayer D, Ruppert M, Korkmaz-Icöz S, Kókény G, Horváth EM, Szabó G, Merkely B, Radovits T. The soluble guanylate cyclase activator cinaciguat prevents cardiac dysfunction in a rat model of Type-1 diabetes mellitus. *Cardiovasc Diabetol* 2015;**14**:145.
52. Hanna R, Nour-Eldine W, Saliba Y, Dagher-Hamalian C, Hachem P, Abou-Khalil P, Mika D, Varin A, El Hayek MS, Pereira L, Farès N, Vandecasteele G, Abi-Gerges A. Cardiac phosphodiesterases are differentially increased in diabetic cardiomyopathy. *Life Sci* 2021;**283**:119857.
53. Xue M, Li Z, Wang Y, Chang Y, Cheng Y, Lu Y, Liu X, Xu L, Li X, Yu X, Sun B, Chen L. Empagliflozin prevents cardiomyopathy via sGC-cGMP-PKG pathway in Type 2 diabetes mice. *Clin Sci (Lond)* 2019;**133**:1705–1720.
54. Zile MR, O'Meara E, Claggett B, Prescott MF, Solomon SD, Swedberg K, Packer M, McMurray JJV, Shi V, Lefkowitz M, Rouleau J. Effects of sacubitril/valsartan on



- biomarkers of extracellular matrix regulation in patients with HFrEF. *J Am Coll Cardiol* 2019;**73**:795–806.
55. Nakagawa H, Kumazawa T, Onoue K, Nakada Y, Nakano T, Ishihara S, Minamino N, Hosoda H, Iwata N, Ueda T, Seno A, Nishida T, Soeda T, Okayama S, Watanabe M, Kawakami R, Saito Y. Local action of neprilysin exacerbates pressure overload induced cardiac remodeling. *Hypertension* 2021;**77**:1931–1939.
  56. Pavo IJ, Pavo N, Kastner N, Traxler D, Lukovic D, Zlabinger K, Spannbauer A, Riesenhuber M, Lorant D, Bartko PE, Goliasch G, Hülsmann M, Winkler J, Gyöngyösi M. Heart failure with reduced ejection fraction is characterized by systemic NEP down-regulation. *JACC Basic Transl Sci* 2020;**5**:715–726.
  57. Lyle MA, Iyer SR, Redfield MM, Reddy YNV, Felker GM, Cappola TP, Hernandez AF, Scott CG, Burnett JC, Pereira NL. Circulating neprilysin in patients with heart failure and preserved ejection fraction. *JACC Heart Fail* 2020;**8**:70–80.
  58. Gheibi S, Kashfi K, Ghasemi A. A practical guide for induction of Type-2 diabetes in rat: incorporating a high-fat diet and streptozotocin. *Biomed Pharmacother* 2017;**95**: 605–613.
  59. Skovso S. Modeling Type 2 diabetes in rats using high fat diet and streptozotocin. *J Diabetes Investig* 2014;**5**:349–358.
  60. Prickett TCR, Lewis LK, Pearson JF, Espiner EA. Metabolism of natriuretic peptides and impact on insulin resistance and fat mass in healthy subjects. *Clin Biochem* 2025;**136**: 110893.
  61. Carper D, Lac M, Coue M, Labour A, Märten A, Banda JAA, Mazeyrie L, Mechta M, Ingerslev LR, Elhadad M, Petit JV, Maslo C, Monbrun L, Del Carmine P, Sainte-Marie Y, Bourlier V, Laurens C, Mithieux G, Joannis DR, Coudray C, Feillet-Coudray C, Montastier E, Viguerie N, Tavernier G, Waldenberger M, Peters A, Wang-Sattler R, Adamski J, Suhre K, Gieger C, Kastenmüller G, Illig T, Lichthagen R, Seissler J, Mounier R, Hiller K, Jordan J, Barrès R, Kuhn M, Pesta D, Moro C. Loss of atrial natriuretic peptide signaling causes insulin resistance, mitochondrial dysfunction, and low endurance capacity. *Sci Adv* 2024;**10**:eadl4374.
  62. Gladysheva IP, Sullivan RD, Reed GL. Falling corin and ANP activity levels accelerate development of heart failure and cardiac fibrosis. *Front Cardiovasc Med* 2023;**10**:1120487.
  63. Petrain A, Nogales C, Krahn T, Mücke H, Lüscher TF, Fischmeister R, Kass DA, Burnett JC, Hobbs AJ, Schmidt HHHW. Cyclic GMP modulating drugs in cardiovascular diseases: mechanism-based network pharmacology. *Cardiovasc Res* 2022;**118**:2085–2102.
  64. Blanton RM. cGMP signaling and modulation in heart failure. *J Cardiovasc Pharmacol* 2020;**75**:385–398.
  65. Ma Y, Li W, Liu Y, Li L. Empagliflozin combined with sacubitril/valsartan in hypertensive patients with heart failure: a retrospective study of efficacy and effect on blood pressure variability and cardiac function. *Am J Transl Res* 2024;**16**:3036–3045.
  66. Jiang J, Gao J, Zhang X, Li Y, Dang H, Liu Y, Chen W. Combined treatment with sacubitril/valsartan plus dapagliflozin in patients affected by heart failure with reduced ejection fraction. *Front Cardiovasc Med* 2023;**10**:1097066.
  67. Karabulut U, Keskin K, Karabulut D, Yiğit E, Yiğit Z. Effect of sacubitril/valsartan combined with dapagliflozin on long-term cardiac mortality in heart failure with reduced ejection fraction. *Angiology* 2022;**73**:350–356.
  68. Mo X, Lu P, Yang X. Efficacy of sacubitril-valsartan and SGLT2 inhibitors in heart failure with reduced ejection fraction: a systematic review and meta-analysis. *Clin Cardiol* 2023;**46**:1137–1145.